

# FOSL1 promotes metastasis of head and neck squamous cell carcinoma through super-enhancer-driven transcription program

Ming Zhang,<sup>1,2,11</sup> Rosalie G. Hoyle,<sup>3,11</sup> Zhikun Ma,<sup>3</sup> Bo Sun,<sup>3</sup> Weixin Cai,<sup>3</sup> Hongshi Cai,<sup>1,2</sup> Nan Xie,<sup>2,4</sup> Yadong Zhang,<sup>1,2</sup> Jinsong Hou,<sup>1,2</sup> Xiqiang Liu,<sup>5</sup> Demeng Chen,<sup>6</sup> Glen E. Kellogg,<sup>3,7</sup> Hisashi Harada,<sup>8,9,10</sup> Yue Sun,<sup>8,9,10</sup> Cheng Wang,<sup>1,2</sup> and Jiong Li<sup>3,7,8,9,10</sup>

<sup>1</sup>Department of Oral and Maxillofacial Surgery, Hospital of Stomatology, Guanghua School of Stomatology, Sun Yat-sen University, Guangzhou 510055, China;

<sup>2</sup>Guangdong Provincial Key Laboratory of Stomatology, Sun Yat-sen University, Guangzhou 510080, China; <sup>3</sup>Department of Medicinal Chemistry, School of Pharmacy, Virginia Commonwealth University, Richmond, VA 23298-0540, USA; <sup>4</sup>Department of Oral Pathology, Hospital of Stomatology, Guanghua School of Stomatology, Sun Yat-sen University, Guangzhou 510055, China; <sup>5</sup>Department of Oral and Maxillofacial Surgery, Nanfang Hospital, Southern Medical University, Guangzhou 510515, China; <sup>6</sup>Center for Translational Medicine, The First Affiliated Hospital, Sun Yat-sen University, Guangzhou 510080, China; <sup>7</sup>Institute for Structural Biology, Drug Discovery and Development, Virginia Commonwealth University, Richmond, VA 23298-0540, USA; <sup>8</sup>Massey Cancer Center, Virginia Commonwealth University, Richmond, VA 23298-0540, USA; <sup>9</sup>Department of Oral and Craniofacial Molecular Biology, School of Dentistry, Virginia Commonwealth University, Richmond, VA 23298-0540, USA; <sup>10</sup>Philips Institute for Oral Health Research, School of Dentistry, Virginia Commonwealth University, Richmond, VA 23298-0540, USA

**Previously, we discovered that FOSL1 facilitates the metastasis of head and neck squamous cell carcinoma (HNSCC) cancer stem cells in a spontaneous mouse model. However, the molecular mechanisms remained unclear. Here, we demonstrated that FOSL1 serves as the dominant activating protein 1 (AP1) family member and is significantly upregulated in HNSCC tumor tissues and correlated with metastasis of HNSCC. Mechanistically, FOSL1 exerts its function in promoting tumorigenicity and metastasis predominantly via selective association with Mediators to establish super-enhancers (SEs) at a cohort of cancer stemness and pro-metastatic genes, such as SNAI2 and FOSL1 itself. Depletion of FOSL1 led to disruption of SEs and expression inhibition of these key oncogenes, which resulted in the suppression of tumor initiation and metastasis. We also revealed that the abundance of FOSL1 is positively associated with the abundance of SNAI2 in HNSCC and the high expression levels of FOSL1 and SNAI2 are associated with short overall disease-free survival. Finally, the administration of the FOSL1 inhibitor SR11302 significantly suppressed tumor growth and lymph node metastasis of HNSCC in a patient-derived xenograft model. These findings indicate that FOSL1 is a master regulator that promotes the metastasis of HNSCC through a SE-driven transcription program that may represent an attractive target for therapeutic interventions.**

## INTRODUCTION

Head and neck squamous cell carcinoma (HNSCC) is one of the deadliest malignant tumors worldwide, with a 5-year survival rate of roughly 50%.<sup>1</sup> HNSCC is highly invasive and frequently metastasizes to cervical lymph nodes (LN), which leads to relapse and death. The long-term survival rates in patients with HNSCC have not

improved significantly in the past 30 years.<sup>1</sup> Thus, an unmet need still exists to develop more effective therapeutic treatment strategies to halt the metastasis of HNSCC. Human HNSCC metastasis may be determined by a variety of regulatory machineries. Elucidation of the molecular mechanisms governing HNSCC metastasis may provide novel therapeutic approaches for the eradication of HNSCC.

Recent evidence suggests that master transcription factors (TFs), together with bromodomain and extraterminal motif proteins (BETs), Mediators, and elongation factors, establish super-enhancers (SEs) at cell type-determining genes to maintain cell identity and status.<sup>2–4</sup> This concept has also been widely accepted in cancer biology: cancer cells are reliant on the high expression of key oncogenes (e.g., MYC) driven by SEs to maintain their malignant phenotype. SEs are usually enriched with master regulators and TFs, such as the BET family transcriptional coactivators, which recruit the Mediator complex, the Pol II complex, as well as the P-TEFb complex, to mediate transcription initiation and elongation.<sup>5–7</sup> Notably, studies have shown that SEs preferentially regulated the transcription of oncogenes in various cancers that can be selectively inhibited by BET or Cyclin-Dependent Protein Kinase (CDK) inhibitors.<sup>4,7,8</sup> Moreover, targeting SEs has become a widely accepted approach in developing

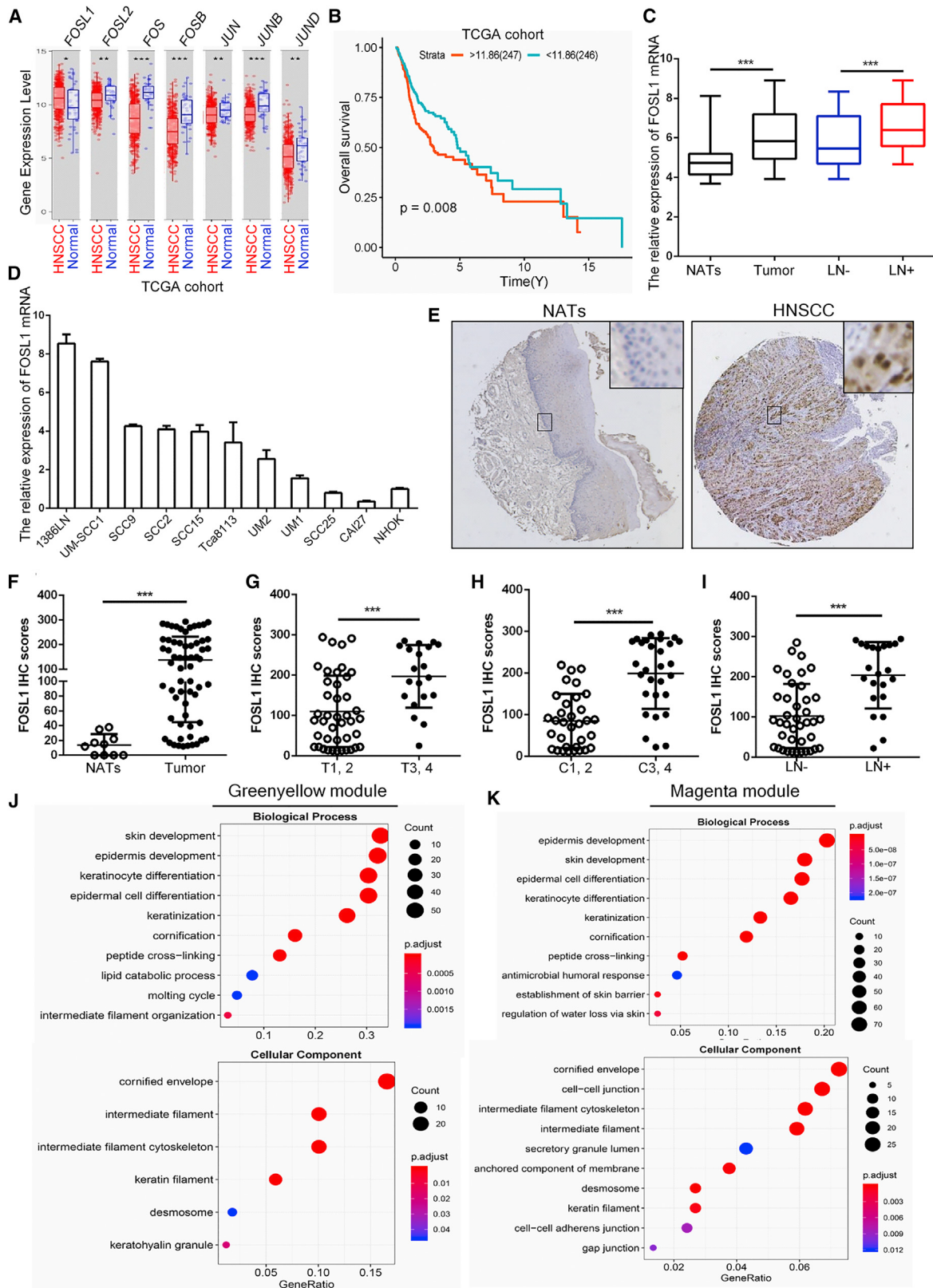
Received 18 July 2020; accepted 25 March 2021;  
<https://doi.org/10.1016/jymthe.2021.03.024>.

<sup>11</sup>These authors contributed equally

**Correspondence:** Jiong Li, PhD, Department of Medicinal Chemistry, School of Pharmacy, Virginia Commonwealth University, Richmond, VA 23298-0540, USA. E-mail: [jli29@vcu.edu](mailto:jli29@vcu.edu)

**Correspondence:** Cheng Wang, MD, DDS, PhD, Department of Oral and Maxillofacial Surgery, Hospital of Stomatology, Guanghua School of Stomatology, Sun Yat-sen University, Guangzhou 510055, China. E-mail: [wangch75@mail.sysu.edu.cn](mailto:wangch75@mail.sysu.edu.cn)





(legend on next page)

new cancer treatment strategies.<sup>7,9</sup> Although BET inhibitors have been widely implemented to target SEs and some effective BET inhibitors are currently in clinical trials for the treatment of several solid tumors (e.g., I-BET-762), BETs also serve as general epigenetic regulators that play critical roles in multiple biological events in normal tissues, including the regulation of chromatin structure, cell cycle control, and stem cell fate determination.<sup>10</sup> In fact, evaluations of ongoing clinical trials reveal that treatment with BET inhibitors is associated with significant toxic side effects, and a comparison of the therapeutic benefit of BET inhibitors to existing therapies is still pending.<sup>11–13</sup> Therefore, additional specific targets need to be identified and new strategies need to be developed to target SEs to overcome the toxic side effects of BET inhibitors in cancer treatment.

AP1 (activating protein 1) is a dimeric transcription factor composed of proteins belonging to the JUN (JUN, JUNB, and JUND), FOS (FOS, FOSB, FOSL1, and FOSL2), and activating transcription factor protein families. Unlike the BET family transcription regulators, the AP1 family TFs are considered to be proto-oncogenes and can be involved in tissue-specific regulation of target genes due to the differential combination of the components of this important TF.<sup>14</sup> AP1 family proteins are well known to promote oncogenesis in various tumors, especially FOSL1 and JUN, which are highly expressed in invasive cancers and can mediate enhanced migration and proliferation.<sup>15–18</sup> FOSL1 has been reported to be associated with malignant phenotypes of HNSCC.<sup>18,19</sup> In agreement with these findings, our previous study also indicated that increased FOSL1 activity mediates the invasive growth and metastasis of Bmi1<sup>+</sup> cancer stem cells (CSCs) in a spontaneous mouse HNSCC model.<sup>20</sup> However, the molecular mechanisms of FOSL1 in maintaining cancer stemness and driving malignant progression of HNSCC remain poorly understood.

In the present study, we discovered that FOSL1 is a dominant AP1 family member that is markedly upregulated and correlated with malignant progression in HNSCC. Mechanistically, FOSL1 exerts its function in promoting tumorigenicity and metastasis of HNSCC predominantly through establishing SEs at a cohort of cancer stemness and pro-metastasis genes, such as *SNAI2* and *FOSL1* itself. Using a human HNSCC patient-derived xenograft (PDX) model, we demonstrated that targeting this FOSL1-SE-driven transcription program profoundly suppresses the expression of these key oncogenes, resulting in the inhibition of tumorigenesis and metastasis of HNSCC. Taken together, our results suggest that FOSL1 is a master regulator of HNSCC and targeting the FOSL1-SE-driven transcription program

can significantly suppress the tumorigenic potential and the metastatic ability of HNSCC.

## RESULTS

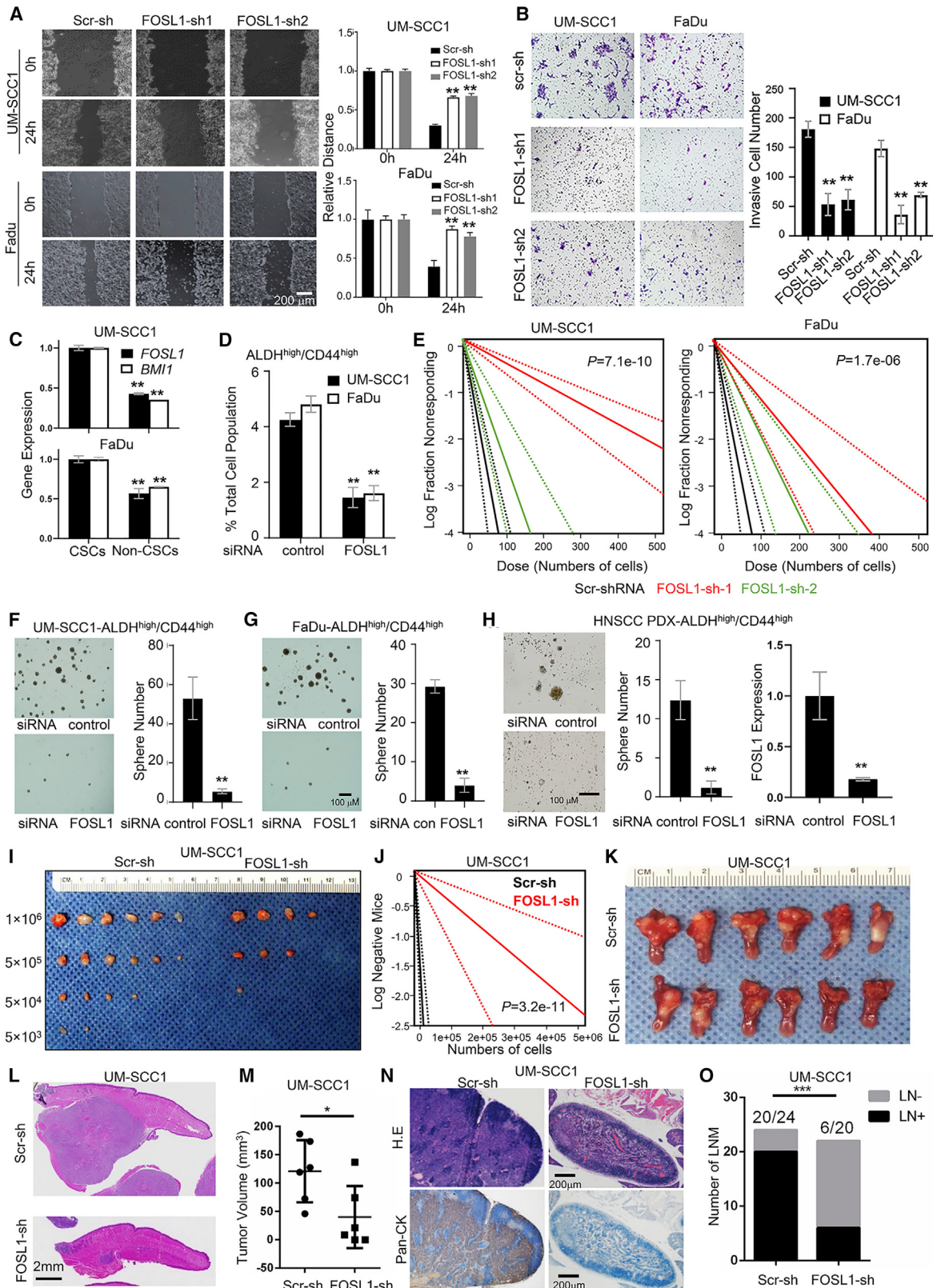
### **FOSL1 is upregulated in HNSCC and is associated with malignant progression of HNSCC**

To investigate whether FOSL1 plays a critical role in human HNSCC progression, we first characterized the mRNA profiles of the HNSCC patient cohort from TCGA. The analysis of the TCGA database revealed that among all detected JUN and FOS family members, FOSL1 mRNA was the only one that was significantly upregulated in the HNSCC samples compared with normal tissues (Figure 1A). Importantly, high expression of FOSL1 mRNA indicates a poor overall survival in the TCGA HNSCC patient cohort (Figure 1B). Furthermore, we comparatively analyzed mRNA profiles by using our HNSCC patient samples ( $n = 53$ ) and their corresponding non-cancerous adjacent tissues (NATs) ( $n = 22$ ).<sup>21</sup> As shown in Figure 1C, the microarray analysis indicates that FOSL1 is significantly upregulated in HNSCC tumor tissues compared with NATs. Of note, FOSL1 expression level is also significantly higher in HNSCC patients with LN metastasis than in those without. We also examined the expression of FOSL1 in a panel of 9 HNSCC cell lines. As expected, FOSL1 is also significantly increased in (7 of 9) HNSCC cell lines compared with normal human oral keratinocyte cells (NHOKs) (Figure 1D). To further validate these findings, a HNSCC tissue microarray (TMA) was employed to analyze the expression of FOSL1 in HNSCC tissues (10 NATs and 65 HNSCC). The results shown in Figures 1F and S1A confirmed that the expression of FOSL1 protein was also dramatically increased in HNSCC compared with NATs. More importantly, FOSL1 protein expression was positively associated with tumor size (T), clinical stage (C), and LN metastasis in HNSCC (Figures 1G–1I). Collectively, our data suggest that FOSL1 is markedly upregulated and is associated with malignant progression of HNSCC.

Next, to investigate the potential biological process in which FOSL1 is involved during the progression of HNSCC, weighted gene correlation network analysis (WGCNA) was performed to explore the key gene modules related to FOSL1 expression. HNSCC samples from TCGA were clustered with respect to FOSL1 expression level (Figure S1B), and a soft threshold of  $\beta = 6$  was selected to obtain the neighboring and topology (Figure S1C). The topological overlap of the gene networks was visualized via a heatmap (Figure S1D), and the clustering tree was divided into 17 modules by dynamic shearing (Figures S1E and S1F). Then, we found that the greenyellow and

**Figure 1. Upregulation of FOSL1 is correlated with malignant progression of HNSCC**

(A) Analysis of AP1 family member expression in 44 normal and 524 HNSCC samples based on the TCGA database from TIMER2.0 (<http://timer.cistrome.org/>). (B) Kaplan-Meier curves for survival of patients with HNSCC grouped by the expression of FOSL1 from the TCGA database. Differences between the two groups were compared with a log-rank test. (C) Analysis of FOSL1 expression using the data sets with 22 normal and 53 HNSCC samples based on the method from our previous study. LN–, negative lymph node metastasis; LN+, positive lymph node metastasis. \*\*\* $p < 0.001$  by Student's t test. (D) qRT-PCR analysis of FOSL1 expression in a panel of 9 HNSCC cell lines compared with NHOK. (E) Representative images of FOSL1 IHC staining of NATs and HNSCC samples from TMA. (F) Analysis of FOSL1 expression in 10 NATs and 64 HNSCC samples from TMA. (G–I) HNSCC samples were grouped by T stage (G), clinical stage (H), and lymph node metastasis (I). \*\*\* $p < 0.001$  by Student's t test. (J and K) GO analysis for genes in greenyellow (J) and magenta (K) modules.



(legend on next page)

magenta modules were most significantly associated with FOSL1 expression (Figure S1G). Gene Ontology (GO) analysis revealed that enrichments of genes in both modules were significantly associated with keratinocyte differentiation in the biological process (BP) classification and intermediate filament cytoskeleton in the cellular component classification (Figures 1J and 1K). Accumulating evidence suggests that cancer cells with high metastatic potentials display a de-differentiated status, including tumor budding cells<sup>22–24</sup> and cancer cells located at the invasive tumor front.<sup>22–24</sup> Importantly, epithelial-mesenchymal transition (EMT), a well-known program required for metastasis, is actually a complex de-differentiation process.<sup>25,26</sup> Moreover, it has been confirmed that rearrangement of the cytoskeleton is required in migration and invasion of cancer cells, which are the key steps of cancer metastasis and phenotype changes from EMT.<sup>27–29</sup> All these findings emphasize that the key biological function of FOSL1 is its involvement in the metastasis cascade in HNSCC. Taken together, our results suggest that FOSL1 is markedly upregulated and is clearly associated with metastasis of HNSCC.

#### FOSL1 promotes HNSCC metastasis and tumorigenicity of HNSCC

To validate the functional role of FOSL1 in promoting the metastasis phenotype of HNSCC cells *in vitro*, we generated two lentivirus-based short hairpin RNAs (shRNAs; sh1 and sh2) to target two different FOSL1 sequences. Both FOSL1-sh1 and FOSL1-sh2 were able to knock down FOSL1 in HNSCC cell lines UM-SCC1 and FaDu (Figure S2A). As shown in Figures 2A and 2B, depletion of FOSL1 significantly inhibited the migration and invasion of UM-SCC1 and FaDu cells. To rule out the possibility that the inhibition of migration was mediated by suppression of cell proliferation, we treated the cells with mitomycin C and performed similar wound healing assays. As shown in Figure S2B, depletion of FOSL1 still significantly suppressed the migration when the proliferation was inhibited.

Since CSCs have been suggested to maintain cancer growth and promote metastasis, the expression of FOSL1 was evaluated in FAC-Sorted ALDH<sup>high</sup>/CD44<sup>high</sup> CSC-like cells from UM-SCC1 and FaDu cells to clarify the critical role of FOSL1 in maintaining the CSCs of HNSCC.<sup>30</sup> Unsurprisingly, significant upregulation of both

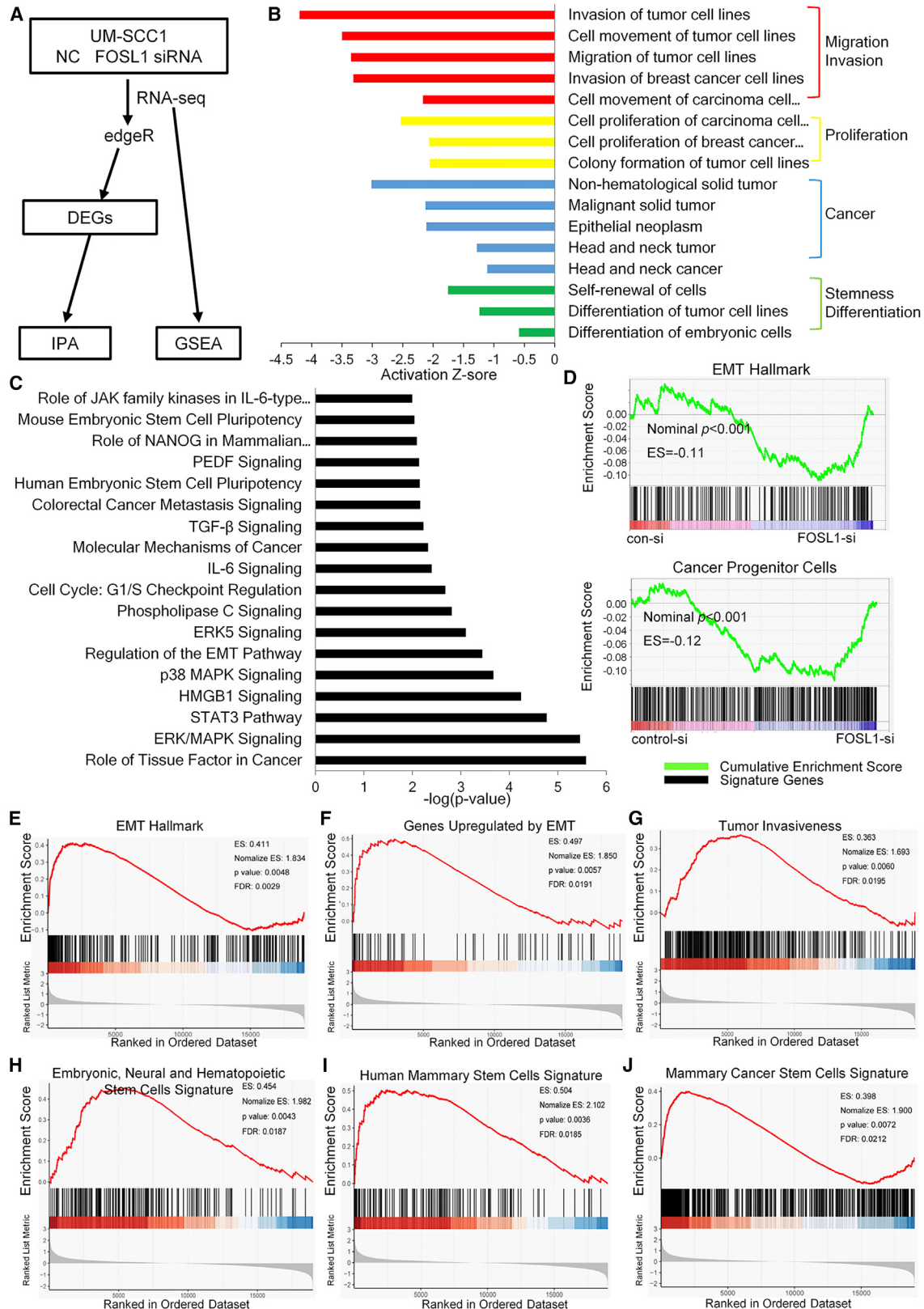
FOSL1 and BMI1 expression was detected in ALDH<sup>high</sup>/CD44<sup>high</sup> CSC-like cells compared with ALDH<sup>low</sup>/CD44<sup>low</sup> non-CSCs (Figure 2C), suggesting that FOSL1 may play an important role in CSC regulation in HNSCC. Supporting this, a reduction of ALDH<sup>high</sup>/CD44<sup>high</sup> CSC population was observed in UM-SCC1 and FaDu cells transfected with FOSL1 small interfering RNA (siRNA) (Figure 2D; Figures S2C and S2D), indicating that the self-renewal capacity of CSCs was impaired by depletion of FOSL1.

To further address whether FOSL1 promotes self-renewal ability in HNSCC *in vitro*, we performed the widely used *in vitro* tumor sphere formation assay but used limiting dilution to ensure the accuracy of measurement. Four doses (1,000, 500, 50, and 10) of the control, FOSL1-sh1, and FOSL1-sh2 UM-SCC1 cells were seeded in 96-well plates. Notably, a significant decrease in the sphere re-initiating cell frequency was detected in the UM-SCC1/FOSL1-sh1 cells as compared to controls (Figure 2E; Figure S2E). Similar results were also observed in FaDu cells (Figure 2E; Figure S2E). For further confirmation, ALDH<sup>high</sup>/CD44<sup>high</sup> CSCs were isolated from both UM-SCC1 and FaDu cells and treated with FOSL1 siRNA. As shown in Figures 2F and 2G, tumor sphere formation was completely abolished by depletion of FOSL1, indicating its pivotal role in maintaining CSC-like self-renewal in HNSCC. In addition, knockdown of FOSL1 dramatically reduced the tumor sphere formation ability of ALDH<sup>high</sup>/CD44<sup>high</sup> CSCs isolated from one case of HNSCC PDX originating from the oral cavity (Figure 2H). These results suggested that FOSL1 plays a key role in the cancer-initiating capacity of HNSCC.

To determine whether FOSL1 promotes tumorigenesis of HNSCC cells *in vivo*, a limiting-dilution assay was also performed and four doses ( $10^6$ ,  $5 \times 10^5$ ,  $5 \times 10^4$ , and  $5 \times 10^3$ ) of UM-SCC1/FOSL1-sh1 cells and their corresponding control cells were subcutaneously inoculated in nude mice. UM-SCC1/FOSL1-sh1 cells displayed lower tumorigenicity (Figure 2I) and tumor re-initiating cell frequency compared with control cells (Figure 2J). Of particular note, the UM-SCC1/FOSL1-sh1 cells could not form visible tumors when  $5 \times 10^3$  cells were injected, suggesting that FOSL1 promotes the CSC population in HNSCC cells. To investigate the pivotal role of

**Figure 2. FOSL1 promotes HNSCC migration, invasive growth, and tumorigenicity of HNSCC**

(A) Depletion of FOSL1-inhibited cell motility of UM-SCC1 and FaDu cells as shown by wound healing assays. \*\*p < 0.01 by one-way ANOVA. Scale bar, 200  $\mu$ m. (B) Depletion of FOSL1-inhibited cell migration and invasion of UM-SCC1 and FaDu cells. \*\*p < 0.01 by one-way ANOVA. (C) qRT-PCR showed that FOSL1 and BMI1 expression was increased in ALDH<sup>high</sup>/CD44<sup>high</sup> cancer stem cells (CSCs) from HNSCC compared with ALDH<sup>low</sup>/CD44<sup>low</sup> non-CSCs. \*\*p < 0.01 by Student's t test. (D) ALDH<sup>high</sup>/CD44<sup>high</sup> CSC population was decreased in UM-SCC1 and FaDu cells treated with FOSL1 siRNA. \*\*p < 0.01 by Student's t test. (E) CSC frequency of FOSL1-sh1, FOSL1-sh2, or Scr-sh transduced HNSCC cells was measured by limiting dilution assay *in vitro*. Frequency and probability estimates were computed with ELDA software. (F and G) Depletion of FOSL1 by siRNA eliminated tumor sphere formation ability of ALDH<sup>high</sup>/CD44<sup>high</sup> CSCs from UM-SCC1 (F) and FaDu (G) cells. \*\*p < 0.01 by Student's t test. Scale bar, 100  $\mu$ m. (H) Depletion of FOSL1 by siRNA eliminated tumor sphere formation ability of tumor cells isolated from HNSCC PDX. The knockdown efficiency of FOSL1 was determined by qRT-PCR. \*\*p < 0.01 by Student's t test. Scale bar, 100  $\mu$ m. (I) *In vivo* limiting dilution analysis of UM-SCC1/FOSL1-sh-1 and UM-SCC1/Scr-sh cells. (J) CSC frequency of UM-SCC1/FOSL1-sh-1 and UM-SCC1/Scr-sh cells was measured by limiting dilution assay *in vivo*. Frequency and probability estimates were computed with ELDA software. (K) HNSCC orthotopic xenograft inoculated with the UM-SCC1/FOSL1-sh1 or UM-SCC1/Scr-sh cells (n = 6 each group). White areas of the tongues represent the xenograft tumors. (L) Representative images of histopathological analysis of the tumor. Scale bar, 2 mm. (M) Tumor volume was suppressed in mice bearing UM-SCC1/FOSL1-sh-1 cells compared with UM-SCC1/Scr-sh cells control cells. n = 6, \*p < 0.05 by Student's t test. (N) H&E and immunostaining of metastatic cells in cervical lymph nodes using anti-pan-cytokeratin (Pan-CK). Scale bar, 200  $\mu$ m. (O) The percentage of lymph nodes with metastatic tumor cells was analyzed by Fisher's exact test. \*\*\*p < 0.001. Values are mean  $\pm$  SD for triplicate samples from a representative experiment, unless otherwise indicated.



(legend on next page)

FOSL1 in promoting metastasis *in vivo*, a HNSCC orthotropic xenograft model was established with UM-SCC1/FOSL1-sh1 cells and their corresponding control cells (UM-SCC1/scrambled shRNA [Scr-sh]). As shown in Figures 2K–2M, mice bearing UM-SCC1/FOSL1-sh1 cells displayed smaller tumors with lower tumor volume than the mice bearing control cells. Moreover, histological analysis revealed that the LN metastasis was also significantly suppressed by depletion of FOSL1 (Figures 2N and 2O). In addition, we also confirmed that depletion of FOSL1 also significantly suppressed tumorigenicity, *in vivo* growth, and the metastatic ability of FaDu cells (Figures S2G–S2M). Overall, these findings confirmed that FOSL1 serves as a key oncogene that promotes the tumorigenesis and metastasis of HNSCC *in vivo*.

#### **FOSL1 promotes epithelial-mesenchymal transition and maintains stemness in HNSCC**

To understand the molecular mechanisms of FOSL1 in promoting HNSCC tumorigenesis and metastasis, RNA sequencing (RNA-seq) was conducted by using HNSCC cells transfected with FOSL1 and control siRNA, followed by Ingenuity Pathway Analysis (IPA) and gene set enrichment analysis (GSEA) (Figure 3A). As shown in Figure 3B, IPA revealed that cell migration, invasion, proliferation, and differentiation were all significantly inactivated by depletion of FOSL1 in UM-SCC1 cells. In agreement with these functional alterations, several key signaling pathways were significantly changed after FOSL1 knockdown, including the EMT pathway, metastasis, stemness, and cell cycle regulation signaling (Figure 3C). These results indicate that FOSL1 plays an essential role in maintaining cancer stemness and EMT in HNSCC. To further confirm these observations, GSEA was employed to analyze the RNA-seq profiles and indicated that depletion of FOSL1 significantly suppresses the EMT signature and cancer stemness signature gene expression (Figure 3D). Similar results were observed in FaDu cells (Figures S3A–S3D).

It is well known that EMT promotes CSC phenotype in many tumor entities.<sup>31,32</sup> To further confirm that FOSL1 regulates EMT, we examined the effect of FOSL1 knockdown on the expression of EMT markers E-cadherin (CDH1) and N-cadherin (CHD2) in both UM-SCC1 and FaDu cells. As shown in Figure S2A, the expression of epithelial marker CDH1 was not very dramatically upregulated by FOSL1 depletion. In comparison, the mesenchymal marker CDH2 expression was significantly reduced. Additionally, knockdown of FOSL1 did not cause significant changes in the morphology of the two cells (Figure S3E). This suggests that FOSL1 may mainly regulate partial EMT.<sup>32</sup> It was recently recognized that the human carcinomas usually undergo partial EMT, rather than complete EMT, possessing a higher metastatic risk.<sup>33</sup> The critical role of partial EMT in domi-

nating HNSCC metastasis has already been confirmed by the single-cell RNA-seq analysis of HNSCC patient tissues.<sup>34</sup> More importantly, we also performed GSEA with the TCGA HNSCC data set. As shown in Figures 3E–3J, we found that the FOSL1 level was positively correlated with EMT and CSC signature genes, supporting the notion that FOSL1 has a crucial role in metastasis and stemness of HNSCC. Taken together, these data indicate that FOSL1 promotes EMT signaling and maintains CSCs in HNSCC.

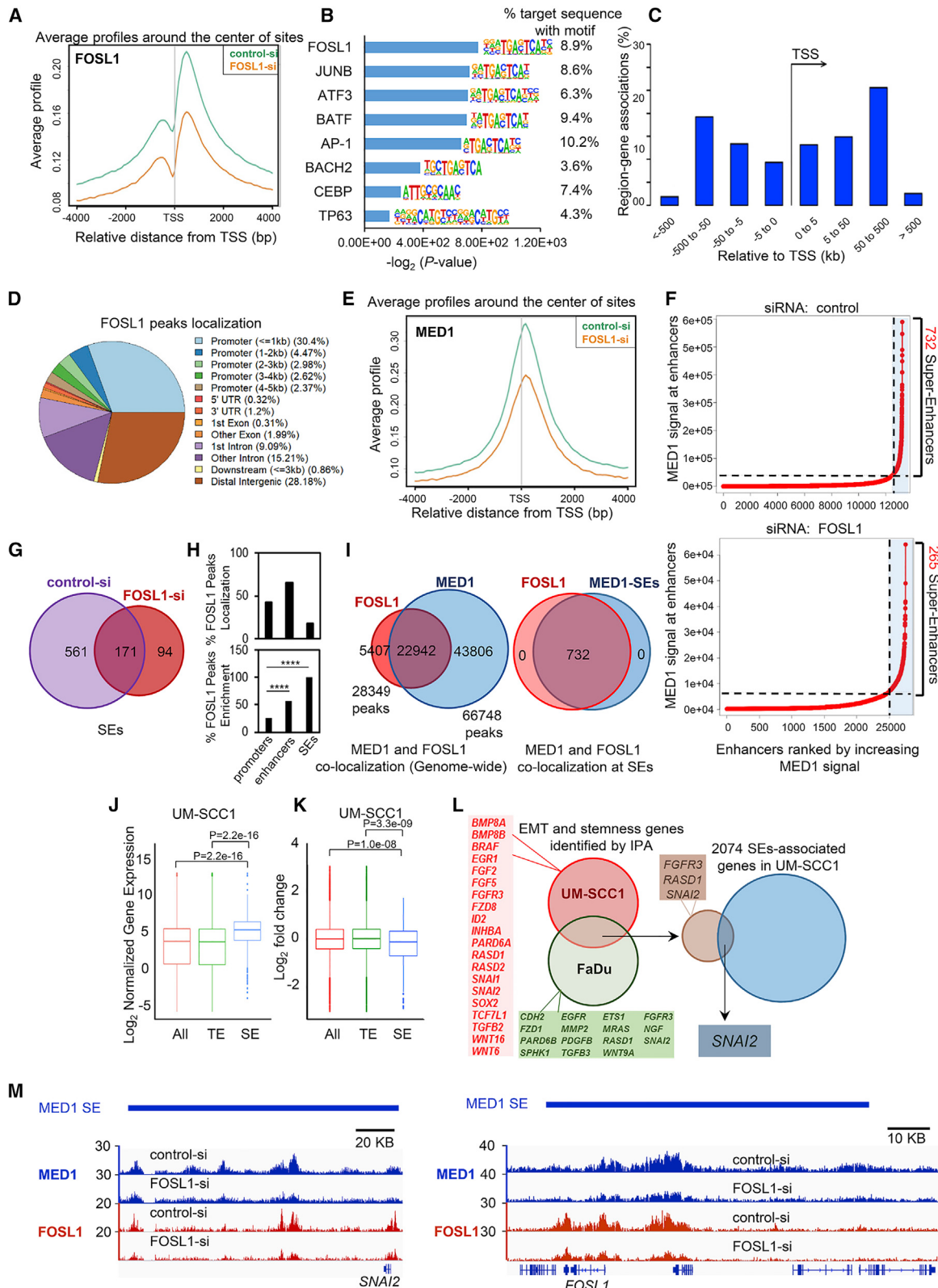
#### **FOSL1 associates with Mediators to establish super-enhancers**

To elucidate the molecular mechanism by which FOSL1 maintains CSCs and metastatic ability of HNSCC, we performed chromatin immunoprecipitation sequencing (ChIP-seq) and examined the genome-wide occupancy of FOSL1 in UM-SCC1 cells following FOSL1 depletion. As expected, a dramatic decrease of FOSL1 occupancy was observed at  $\pm 5$  kb from the transcription start site (TSS), the promoter regions, in FOSL1-depleted UM-SCC1 cells (Figure 4A). We identified 28,349 FOSL1-occupied regions (peaks) on chromatin in control UM-SCC1 cells genome-wide. Transcription factor DNA motif analysis also confirmed that AP1 family member binding motifs are significantly enriched in FOSL1 peak regions, and FOSL1 motif is identified at the top of the list (Figure 4B). Interestingly, the majority of these regions were found  $\pm 5$  kb away from the TSS, particularly  $\pm 50$ –500 kb away from the TSS (Figure 4C). Globally, analysis of the distribution of FOSL1-occupied regions relative to annotated TSSs revealed that most FOSL1 peaks were intragenic and intergenic sites located distally from the promoter (Figure 4D). This suggests that instead of promoter regions, FOSL1 may predominantly associate with the enhancer regions in HNSCC cells.

Recent evidence suggests that master TFs recruit Mediators to establish SEs at the key cell identity genes that determine cell type and identities.<sup>2,7</sup> Based on our results, we hypothesize that FOSL1 may exert its function in promoting metastasis and stemness in HNSCC by establishing SEs with Mediators. To test this hypothesis, we also performed the ChIP-seq of Mediator complex subunit MED1 and characterized the SEs in UM-SCC1 cells after FOSL1 depletion in parallel. As shown in Figure 4E, a dramatic reduction of MED1 enrichment on chromatin was also observed in the FOSL1-depleted UM-SCC1 cells. When defined by the ChIP signal of MED1, 732 SEs were identified in control cells and only 265 were identified in FOSL1-knockdown cells (Figure 4F). Among the 732 SEs identified in control cells, 561 of them were lost in FOSL1-depleted cells (Figure 4G). A genome-wide analysis confirmed that a considerable number of the FOSL1 peaks (18.6%) were distributed to the SE regions (Figure 4H). The analysis also indicated that the ratio of SEs (100%) that contain FOSL1 peaks is significantly higher than

#### **Figure 3. FOSL1 promotes EMT and cancer stemness in HNSCC**

(A) Schematic illustrating the experimental approach for RNA-seq and subsequent data analysis in UM-SCC1 cells. (B) IPA showed that FOSL1 target genes are associated with proliferation, migration, invasion, and stemness. (C) IPA demonstrated that FOSL1 target genes are enriched in metastasis- and stemness-associated signaling. (D) GSEA indicated that the depletion of FOSL1 inhibits the EMT and cancer progenitor cell signature genes.  $p < 0.001$ . (E–J) GSEA indicated that the abundance of FOSL1 is positively correlated with EMT (E), EMT upregulated genes (F), tumor invasiveness (G), embryonic, neural, and hematopoietic stem cells (H), human mammary stem cells (I), and mammary cancer stem cells signature (J) gene expression in HNSCC samples from the TCGA database.



(legend on next page)

promoter (25.1%) and the enhancer regions (57.0%) (Figure 4H). To further validate our hypothesis, we characterized both FOSL1 and MED1 chromatin localization with ChIP-seq. Among the 28,349 FOSL1-occupied region and 66,748 MED1-occupied region sites, 22,942 sites were shared by both FOSL1 and MED1. Among the 732 SEs identified based on MED1 enrichment, 100% contained potential binding sites for FOSL1 (Figure 4I). An endogenous nuclear IP analysis in UM-SCC1 also confirmed the interaction between FOSL1 and MED1 in the nucleus (Figure S4A). Taken together, our data suggest that FOSL1 is significantly enriched at SEs and selectively co-localizes with MED1 to establish SEs in SCC cells.

An emerging paradigm in cancer biology relates to the concept of “transcriptional addiction: to support their uncontrolled proliferation or other needs, tumor cells require high levels of uninterrupted transcription of a large set of genes to sustain their malignant phenotypes.”<sup>35,36</sup> These key oncogenes are usually driven by SEs, and they are vulnerable to SE disruption.<sup>37</sup> Therefore, we asked whether SE-associated transcripts are more disproportionately relying on FOSL1 than typical enhancers (TEs). An analysis of transcriptional profiles indicated that SE-associated transcripts were significantly more expressed than TE-associated transcripts (Figure 4J). In addition, the abundance of SE-associated transcripts was downregulated to a significantly higher degree upon depletion of FOSL1 compared with those associated with TEs (Figure 4K), thus indicating that SE-associated genes are, in particular, transcriptionally addicted to FOSL1.

In order to identify key target genes that promote EMT and cancer stemness controlled by FOSL1-SEs, the EMT and stemness genes identified by RNA-seq and IPA in both UM-SCC1 cells and FaDu cells were merged with 2,074 SE-associated genes, resulting in only one target gene, SNAI2 (Figure 4L). SNAI2, a critical EMT transcriptional factor, has been demonstrated to maintain stemness and promote invasive growth in a wide range of malignancies, including HNSCC.<sup>37,38</sup> Of note, a recent single-cell sequencing analysis of HNSCC tissues also highlighted its decisive role in maintaining the partial EMT program to dominate the malignant progression and metastasis of HNSCC.<sup>34</sup> The evidence suggests that SNAI2 may play a key role in mediating the functions of FOSL1-SEs in HNSCC. To test this hypothesis, we constructed stable SNAI2-overexpressing UM-SCC1 cells and control cells and depleted FOSL1 expression by siRNA (Figure S4B). We found that overexpression of SNAI2 restored the migration and invasion ability reduced by FOSL1 depletion (Fig-

ures S4C and S4D). In addition, the tumor sphere formation ability was also rescued by overexpression of SNAI2 (Figure S4E). Thus, these results indicate that SNAI2 is a key target gene of FOSL1-SE and it may play an essential role in exerting the functional characteristics of FOSL1-SEs in HNSCC.

In addition to SNAI2, we also identified a cohort of cancer stemness genes associated with FOSL1-SEs, such as *CD44*, *EPHA2*, and *FOSL1* itself (Figure 4M; Figures S5A and S5B). *CD44* is a well-known CSC marker in HNSCC,<sup>30</sup> and *EPHA2* has been reported to drive self-renewal and tumorigenicity in stem-like tumor-propagating cells from human glioblastomas.<sup>39</sup> Additionally, other key oncogenic genes that promote tumor growth (*S100A1* and *S100A2*), survival (*MCL1* and *BIRC5*), and metastasis (*MMP3* and *MMP8*) are also associated with FOSL1-SEs (Figures S5C–S5G). The ChIP-seq profiles showed that the signals for MED1 and FOSL1 were highly enriched at the SEs that were significantly reduced after knockdown of FOSL1 (Figure 4M; Figures S5A–S5G). Overall, these results indicate that the FOSL1-SE-driven transcription program plays an essential role in maintaining cancer stemness and metastatic ability of HNSCC.

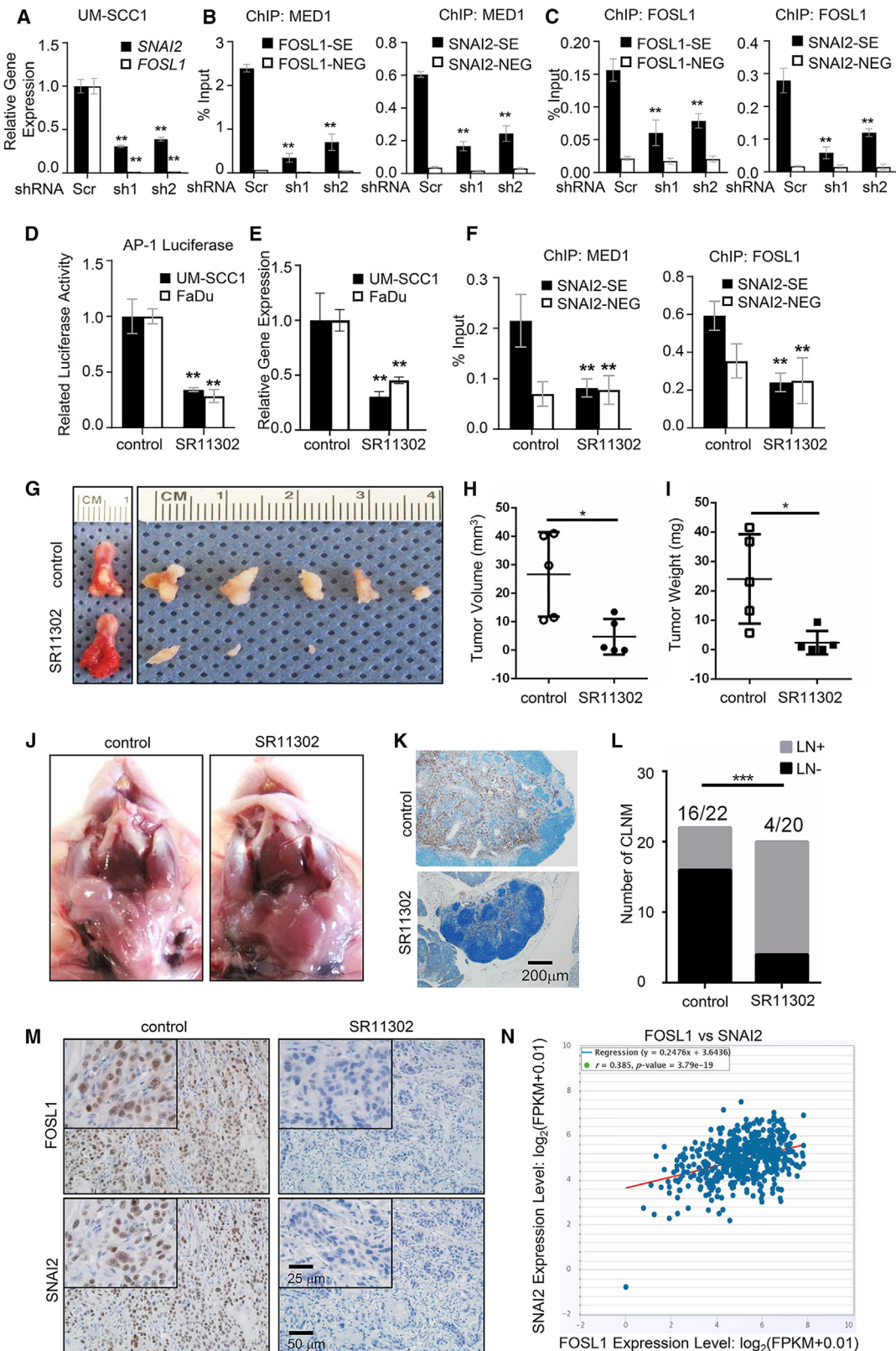
#### Targeting FOSL1 inhibits SE-associated gene expression and suppresses tumor growth and metastasis in HNSCC

To further confirm the relationship of FOSL1 and SE-associated genes, we performed quantitative real-time PCR validation and showed that depletion of FOSL1 by shRNA significantly inhibited the expression of *SNAI2*, *FOSL1*, and other SE-associated genes in HNSCC cells (Figure 5A; Figure S6A). Similar results were also obtained by knockdown of FOSL1 via siRNA in UM-SCC1, FaDu, and tumor cells isolated from PDX (Figures S6B and S6C). ChIP-quantitative real-time PCR confirmed that the enrichments of MED1 and FOSL1 on the SE regions were also significantly decreased after depletion of FOSL1 by both shRNA and siRNA (Figures 5B and 5C; Figures S6D–S6G).

Moreover, we also found that the AP1 inhibitor, SR11302, which has been reported to inhibit the transcriptional activity of AP1 *in vitro* and *in vivo*,<sup>40–45</sup> significantly suppressed AP1 activity (Figure 5D) as well as the expression of *SNAI2*, *FOSL1*, and other SE-associated genes in both UM-SCC1 and FaDu cells (Figure 5E; Figure S6I). Finally, ChIP-quantitative real-time PCR analysis also demonstrated that SR11302 significantly suppresses the recruitment of FOSL1 and MED1 to the SE regions of these genes (Figure 5F; Figure S6J). These

**Figure 4. FOSL1 exerts its functions in maintaining EMT, invasion, and cancer stemness through SEs in HNSCC cells**

(A) FOSL1 occupancies on genome in UM-SCC1 cells treated with FOSL1 siRNA or control siRNA. (B) Motif analysis at FOSL1-binding sites (peaks) in UM-SCC1 cells. Top 8 most enriched transcription factors are presented. (C) The distribution of FOSL1 peaks in relation to the TSS by GREAT analysis in UM-SCC1 cells. (D) Percent genomic distribution of FOSL1 peaks in genome. (E) Depletion of FOSL1 by siRNA decreased the MED1 occupancies on genome in UM-SCC1 cells by ChIP-seq. (F) Depletion of FOSL1 by siRNA disrupted SEs in UM-SCC1 cells based on MED1 enrichment. (G) The majority of SEs were lost by FOSL1 depletion. (H) The genome-wide distribution of FOSL1 peaks and enrichment in promoters, enhancers, and SEs. \*\*\*p < 0.0001 by Fisher's exact test. (I) FOSL1 selectively associated with MED1 to establish SEs in HNSCC cells. (J) Genes associated with SEs display higher expression levels than genes that associated with total pool of all enhancers (All) and typical enhancers (TEs) in UM-SCC1 cells. The expression values (in RPKM) were determined by RNA-seq and are presented as boxplots. (K) Boxplots showing log<sub>2</sub> fold changes for transcripts associated with total pool of all enhancers (All), TEs, and SEs after FOSL1 depletion in UM-SCC1 cells. (L) Venn diagram shows the overlap between genes associated with SEs and EMT and stemness genes identified by IPA after depletion of FOSL1. (M) MED1 and FOSL1 binding profiles of SE-associated genes *SNAI2* and *FOSL1* in UM-SCC1 cells.



(legend on next page)

results highlight that SR11302 may target the FOSL1-SE-driven transcription program and such an approach may have therapeutic potentials in HNSCC treatment.

To forward these findings toward a clinical intervention strategy, a HNSCC PDX orthotopic preclinical model was established, and the PDX-bearing mice were then treated with either SR11302 or control vehicle. As shown in Figure 5G, administration of SR11302 significantly inhibited the HNSCC PDX growth. Both tumor weight and tumor volume were significantly suppressed by the administration of SR11302 (Figures 5H and 5I). To evaluate the effect of SR11302 on suppressing HNSCC cervical LN metastasis, neck dissection was performed to harvest all the cervical LNs, including the submandibular LNs, superficial cervical LNs, facial LNs, and internal jugular LNs. As shown in Figures 5J–5L, the number of LN metastases was significantly reduced by SR11302 treatment. Consistently, histological analysis also indicated that expression of *SNAI2* and *FOSL1* was dramatically inhibited in the mice treated with SR11302 compared with those in the control group (Figure 5M). Toxicology studies were performed using wild-type mice treated with SR11302. Histopathological analysis revealed that no tissue damage occurred in major organs (including the heart, spleen, lung, brain, kidney, and liver) after SR11302 administration (Figure S7A). In addition, the evaluation of blood routine and blood biochemical indicators also suggested that SR11302 is well tolerated by mice (Figures S7B and S7C).

In agreement with these results, a positive correlation of *FOSL1* and *SNAI2* expression was also observed in HNSCC patients from TCGA data sets (Figure 5N). To further investigate the clinical translational significance of *FOSL1* and its controlled SE-associated genes, immunohistochemistry (IHC) staining was used to assess *FOSL1* and *SNAI2* expression in a cohort of HNSCC tissue samples. As shown in Figures 6A–6C, *FOSL1* and *SNAI2* expression was positively associated with advanced T stage, clinical stage, and cervical LN metastasis. A significant correlation of *FOSL1* and *SNAI2* was also observed at protein levels in HNSCC (Figure 6D). Importantly, high expressions of *FOSL1* and *SNAI2* indicated a poor survival in HNSCC (Figures 6E and 6F). Of note, patients with both low *FOSL1* and *SNAI2* levels indicated the most favorable prognosis (Figure 6G). In summary, these findings strongly suggest that targeting *FOSL1* may serve as a novel therapeutic approach in HNSCC by suppressing the SE-dependent transcriptional program.

#### **Figure 5. Targeting FOSL1 suppresses tumorigenesis and metastasis of HNSCC**

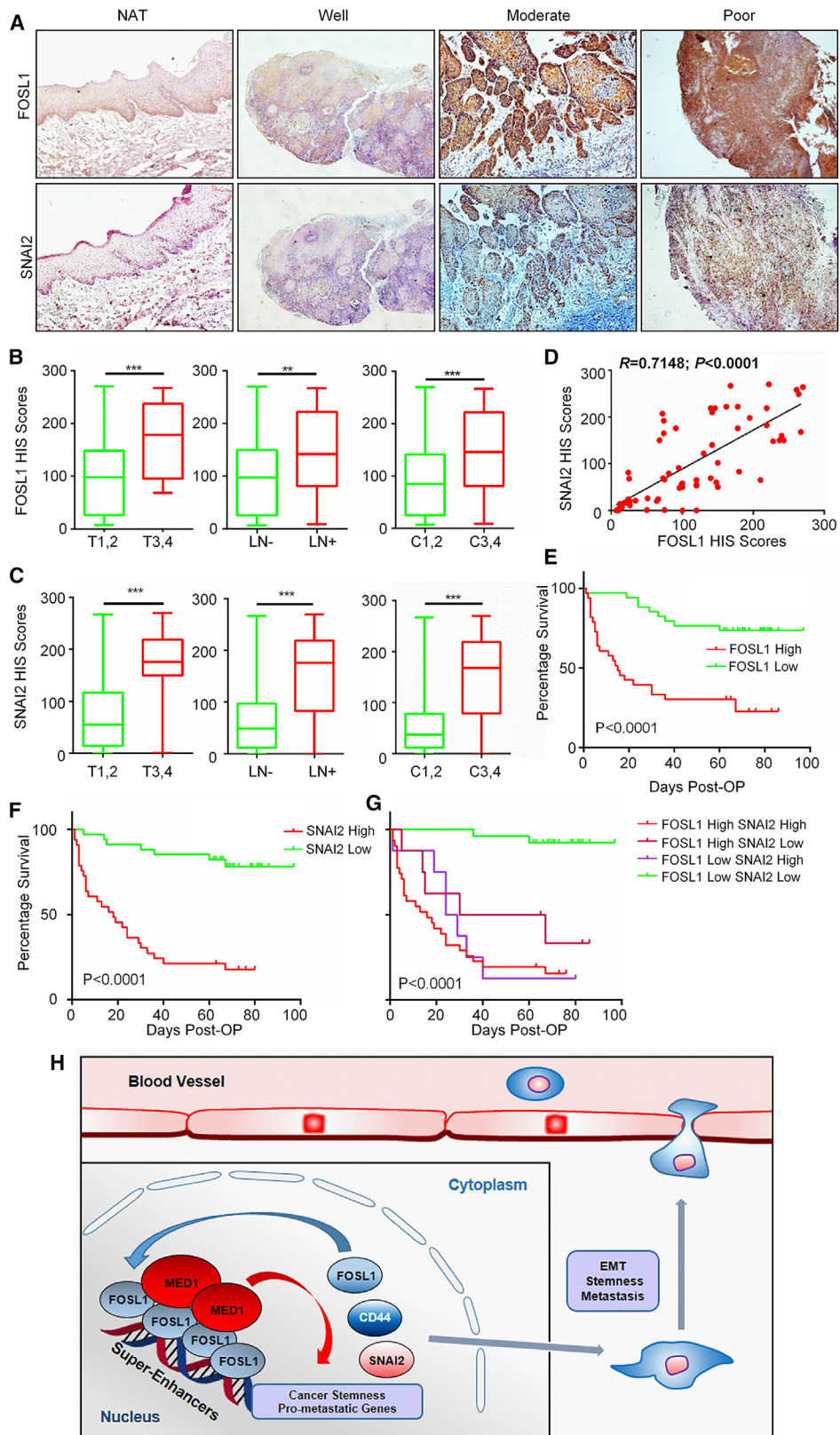
(A) Depletion of *FOSL1* by shRNAs significantly inhibited *SNAI2* expression in UM-SCC1 cells. \*\**p* < 0.01 by Student's t test. (B and C) ChIP-quantitative real-time PCR showed that depletion of *FOSL1* by shRNAs significantly reduced the recruitment of MED1 (B) and *FOSL1* (C) on the SE regions of *SNAI2* and *FOSL1*. (D) SR11302 inhibited AP-1 luciferase activity in UM-SCC1 and FaDu cells. (E) SR11302 inhibited *SNAI2* expression levels in UM-SCC1 and FaDu cells. (F) ChIP-quantitative real-time PCR showed that depletion of *FOSL1* significantly reduced the recruitment of MED1 and *FOSL1* on the SE regions of *SNAI2* in UM-SCC1 cells. (G) Administration of SR11302 inhibited the HNSCC PDX growth *in vivo*. Image of orthotopic PDX treated with SR11302 or control vehicles. (H and I) Quantification of tumor volume (H) and tongue weight with tumor (I) from orthotopic PDX treated with SR11302 or control vehicles. *n* = 5, \**p* < 0.05 by Student's t test. (J) Representative image of cervical lymph node from mice bearing orthotopic PDX treated with SR11302 or control vehicles. (K) Immunostaining of metastatic cells in cervical lymph nodes using Pan-CK. Scale bar, 200  $\mu$ m. (L) The percentage of lymph nodes with metastatic tumor cells was analyzed by Fisher's exact test. \*\*\**p* < 0.001. (M) Administration of SR11302 inhibited *FOSL1* and *SNAI2* expression in HNSCC orthotopic PDX. Immunostaining of HNSCC orthotopic PDX using *FOSL1* and *SNAI2* antibodies. Scale bar top, 25  $\mu$ m; scale bar bottom, 50  $\mu$ m. (N) The abundance of *FOSL1* is positively correlated with *SNAI2* expression in HNSCC samples based on TCGA database from starBase. Values are mean  $\pm$  SD for triplicate samples from a representative experiment, unless otherwise indicated. \**p* < 0.05 and \*\**p* < 0.01 by Student's t test.

#### **DISCUSSION**

Our study uncovered a novel SE-driven transcription mechanism with clinical relevance involving the master regulator *FOSL1* associating with Mediators to establish SEs and thereby promoting tumor initiation and metastasis of HNSCC. Deregulation of transcription is one of the major factors in the propagation of human cancers.<sup>46</sup> This deregulation is often a consequence of mutated and/or overexpressed TFs or epigenetic regulators.<sup>46–48</sup> This results in cancer cells that may be addicted to certain TFs in order to sustain the high expression of select oncogenes and maintain the malignant phenotype.<sup>3,7,35,36,46</sup> We have made an advance in understanding the molecular mechanisms underlying transcriptional addiction in HNSCC cells by identifying *FOSL1* as a relevant player in this phenomenon. The underlying molecular event is mediated by the *FOSL1*-SE-driven transcription program.

The transcriptional activity of the AP1 functions in a tissue-specific or cancer type-specific fashion.<sup>49</sup> By analyzing multiple HNSCC patient cohorts and TCGA database, we found that *FOSL1* is the only AP1 family member that is significantly upregulated in HNSCC tissues and is also correlated with the malignant progression and metastasis of this cancer. Using *in vitro* and *in vivo* models, we further validated its function in promoting tumorigenicity and metastatic ability in HNSCC. In order to investigate the molecular mechanisms underlying these events, we conducted unbiased IPA and GSEA of the RNA-seq and TCGA database and thereby determined that the EMT transcription program and cancer stemness genes are the key mechanisms/targets in mediating tumorigenicity and metastatic function of *FOSL1* in HNSCC. Next, ChIP-seq was performed to identify the comprehensive mechanisms as well as target genes that control these functions. Unexpectedly, we discovered that instead of promoter regions, *FOSL1* was mainly associated with enhancers, especially with SEs. In addition, our data suggested that *FOSL1* may exert its function predominantly through establishing SEs at a cohort of cancer stemness and pro-metastatic genes with preferential association with Mediators. Finally, by overlapping IPA and ChIP, we identified the EMT TF *SNAI2* as the key target gene of *FOSL1*-SEs that control cancer stemness and metastasis.

Emerging evidence from both experimental and clinical studies indicates that EMT promotes tumor initiation, invasion, and



(legend on next page)

metastasis.<sup>32,33</sup> EMT has also been implicated as a critical regulator of CSC phenotype, which includes cancer stemness and metastasis.<sup>31</sup> Multiple molecular signaling, such as the TGF- $\beta$ , Notch, Wnt, and HGF pathways, can regulate the EMT.<sup>33</sup> These signaling pathways often exert their effects on EMT by regulating the expression of key EMT TFs, such as *ZEB1/2*, *TWIST1/2*, *SNAI1*, and *SNAI2*.<sup>50,51</sup> EMT TFs are usually tissue or cancer type specific. Thus, identifying and understanding the cancer type-specific EMT regulatory mechanism may provide more effective strategies for specific cancer types. *SNAI2* is conserved across species and has been demonstrated to play a critical role in maintaining cancer stemness and promoting metastasis in several types of malignancies, especially breast cancer. For example, it has been reported that *SNAI2* is a master regulator that promotes tumorigenic and metastatic abilities of the mammary CSCs.<sup>52</sup> In lung carcinoma, *SNAI2* is also required for SOX9 stabilization and functions to promote CSCs and metastasis.<sup>53</sup> In HNSCC, *SNAI2* has been implicated in sustaining tumor-initiating capacities and metastasis abilities.<sup>21,34,54</sup> Of particular note, a recent analysis of single-cell sequencing of HNSCC patient tissues revealed that a partial EMT program dominantly governs the metastasis of HNSCC, and remarkably *SNAI2* is the only EMT transcriptional factor that was identified to control such an event in HNSCC.<sup>34</sup>

Despite these critical findings, the molecular mechanisms and the transcriptional factors that directly control *SNAI2* expression and promote EMT-governed cancer stemness and metastasis are still not well documented, especially in HNSCC. In addition, an effective method for targeting *SNAI2* has not been developed at present. Here, we identified that FOSL1 establishes SE at *SNAI2* and directly controls its expression. Targeting FOSL1-SEs profoundly suppressed *SNAI2* expression both *in vitro* and *in vivo*. Notably, the suppressed malignant phenotypes, such as the tumor-initiating capacities and invasive growth abilities, in FOSL1-depleted HNSCC cells can be reversed by *SNAI2* overexpression. Importantly, a positive correlation between *FOSL1* and *SNAI2* was also observed in two independent HNSCC patient cohorts. Considering the heterogeneity of the cancer, it is not surprising that some HNSCC patients have high *FOSL1* expression but not *SNAI2* (Figure 6G). Such a phenomenon may be contributed to other factors that can also regulate *SNAI2*. For examples, CD271, nuclear factor- $\kappa$ B (NF- $\kappa$ B), and miR-204-5p have been reported to directly or indirectly regulate *SNAI2* levels in HNSCC.<sup>54–56</sup> However, the statistical analyses of two independent patient cohorts both identified a significantly positive correlation between *FOSL1* and *SNAI2* expression in HNSCC (Figures 5N and 6D), suggesting that this correlation is very robust and convincing. Finally, the evidence that high expression levels of *FOSL1* and *SNAI2* are associated with short over-

all disease-free survival also emphasizes the critical role of the FOSL1-SE/*SNAI2* axis in promoting malignant progression of HNSCC. Taken together, these findings suggest that *SNAI2* is the decisive player in exerting the functional characteristics of FOSL1-SEs, and such a FOSL1-SE/*SNAI2* axis may serve as the master regulatory machinery in promoting HNSCC malignant progression. In addition, our study may also provide a unique strategy for targeting *SNAI2* in HNSCC.

Besides *SNAI2*, other key oncogenic genes that promote tumor invasion (*MMP3* and *MMP12*), stemness (*CD44* and *EPHA2*), growth (*S100A1* and *S100A2*), and survival (*MCL1* and *BIRC5*) have also been identified to be directly controlled by FOSL1-SEs (Figures S5A–S5G). Targeting FOSL1-SEs can also significantly suppress expression of these genes, such as *MCL1* and *MMP3* in HNSCC (Figure S6H). A positive correlation of *FOSL1* and these SE-target gene expressions was also observed in HNSCC patients from TCGA data sets (Figure S6K). Thus, these key oncogenes may also have contributions to the cancer stemness and metastasis functions of FOSL1-SEs. These findings further strengthen the key role of the FOSL1-SE-driven transcription program in maintaining the malignant phenotype of HNSCC. AP1 activity is transcriptionally induced by itself.<sup>57</sup> Likewise, we also found that FOSL1 is directly controlled by FOSL1-SEs. In addition, AP1 members including FOSL1 are well known to be activated by the mitogen-activated protein kinase (MAPK)/extracellular signal-regulated kinase (ERK) pathway, which is also a downstream cascade of *CD44*.<sup>58–60</sup> This suggests that the FOSL1-SE-driven transcription program is sustained by autofeedback loops in which FOSL1 serves as the key hub driver in the center of this signaling network (Figure 6H). Collectively, our discovery indicates that FOSL1 is a master regulator that associates with Mediators to create the FOSL1-SE-driven transcription program through a signaling network to drive the malignant progression of HNSCC.

CSCs are responsible for tumor initiation, metastasis, and drug resistance.<sup>61–63</sup> Targeting CSCs represents a more effective strategy than conventional therapy in cancer treatment. New evidence suggests that SEs may play a critical role in controlling the characteristics of CSCs.<sup>64</sup> Of note, a recent report suggests that CSC-specific SEs promote polyunsaturated fatty acid synthesis to support epidermal growth factor (EGF) receptor (EGFR) signaling to sustain glioma CSCs.<sup>65</sup> This highlights that SEs may define the functional properties of CSCs and targeting SEs may significantly reduce these properties, thereby effectively eliminating CSCs. In agreement with the above-mentioned findings, our studies strongly suggest that the FOSL1-SE-driven transcription program may be required for maintaining

#### Figure 6. The abundance of FOSL1 correlates with poor prognosis in HNSCC

(A) Representative images of IHC analysis of FOSL1 and *SNAI2* expression in HNSCC samples. (B and C) Analysis of FOSL1 (B) and *SNAI2* (C) expression in 67 HNSCC samples. HNSCC samples were grouped by T stage (T1,2 and T3,4), lymph node metastasis (LN– and LN+), and clinical stage (C1,2 and C3,4). Data represent mean  $\pm$  SD. \*\*p < 0.01 and \*\*\*p < 0.001 by Student's t test. (D) The abundance of *FOSL1* is positively correlated with *SNAI2* expression in HNSCC samples. (E and F) Kaplan-Meier curves and log-rank test were used for survival analysis of patients with HNSCC grouped by the expression of *FOSL1* (E) or *SNAI2* (F). (G) Kaplan-Meier curves for survival of patients with HNSCC grouped by the high or low expression of *FOSL1* combined with *SNAI2*. (H) Proposed model for FOSL1-SE transcriptional program in HNSCC progression.

the CSC-like properties, such as self-renewal ability, tumorigenic potential, and metastatic ability, in HNSCC. Indeed, the evidence obtained here and previously shows that FOSL1 is upregulated in HNSCC CSCs compared with non-CSCs, regardless of species.<sup>20</sup> These results strongly imply the critical role of FOSL1-SEs in defining the functional properties of CSCs in HNSCC. Thus, the FOSL1-SE-driven transcription program may serve as a novel and effective therapeutic target for the elimination of CSCs and may be adopted for clinical intervention. However, a question remains of whether the FOSL1-SEs we identified are actually present in CSCs, since these SEs were characterized using the whole population of HNSCC cells. Thus, future studies will be focused on characterization of CSC-specific SEs and validation of their decisive roles in maintaining the functional properties of CSCs in HNSCC.

In conclusion, we have discovered that FOSL1 is a master regulator in HNSCC and it exerts its function in promoting tumorigenicity and metastasis predominantly via establishing SEs at key oncogenes, especially *SNAI2*. We also demonstrated that targeting the FOSL1-SE-driven transcription program may represent an attractive strategy for therapeutic interventions. Collectively, our findings provide not only new insights into the key regulatory mechanisms of cancer stemness and metastasis but also a novel and effective therapeutic approach for eradication of HNSCC, which is still a life-threatening disease without an effective targeted therapeutic strategy at present.

## MATERIALS AND METHODS

### Cell culture and siRNA transfection

The human HNSCC cell lines SCC9, UM-SCC15, SCC25, CAL27, NHOK, and FaDu used in the present study were obtained from ATCC (Rockville, MD, USA). UM-SCC1 cells were obtained from the University of Michigan. 1386LN, UM1, and UM2 cells were provided by Dr. Xiaofeng Zhou (University of Illinois at Chicago, IL, USA). UM-SCC1, CAL27, and FaDu were cultivated in Dulbecco's modified Eagle's medium (DMEM). The SCC9, UM-SCC15, SCC25, UM1, UM2, and 1386LN cells were maintained in DMEM-F12 medium. All the cells were incubated at constant temperature (37°C) in a humidified atmosphere containing 5% CO<sub>2</sub>. The DMEM and DMEM-F12 medium were supplemented with 10% fetal bovine serum (FBS, Thermo Fisher) and 1% penicillin-streptomycin before application to the cell lines. The PlascoTest mycoplasma contamination detection kit (InvivoGen) was utilized to monitor the potential mycoplasma contamination of the cell lines. PLKO.1 lentivectors that express FOSL1-shRNA or Scr-shRNA and packaging vectors were obtained from Horizon. For viral particle productions, lentivirus was obtained by co-transfection of PLKO.1 vectors with packaging plasmids into 293T cells. To establish the FOSL1 knockdown stable cell lines, UM-SCC1 or FaDu cells were incubated with viral particles for 12 h. Two days post virus infection, the cells were selected with puromycin (1 mg/L) for 4 days. The siRNA oligonucleotide sequences were *FOSL1* (si-1: 5'-GCUCAUCGCAAGA GUAGCA-3' and si-2: 5'-GAGCUGCAGUGGAUGGUAC-3'). For siRNA transfection, HNSCC cells were plated at 40%-50% confluence and incubated overnight. The cells were then transfected with various

amounts of siRNA with Lipofectamine RNAiMAX (Life Technologies) according to the manufacturer's instructions.

### Patients and specimens

Two patient cohorts were used in this study, including the HNSCC tissue array and the SYSU HNSCC patient cohort. The HNSCC tissue array (HOraC080PG01) was purchased from Shanghai Outdo Biotech Co. The SYSU HNSCC patient cohort was harvested from 67 patients pathologically diagnosed with HNSCC in the Hospital of Stomatology, Guanghua School of Stomatology, Sun Yat-sen University. The study protocol was submitted and approved by the Ethical Committee of the hospital. None of the patients received chemotherapy or radiotherapy other than a radical surgery. All of the included cases with specific clinicopathological data were then subjected to TNM stage analysis referring to the UICC classification system. The survival time was defined as the period from the surgery date to the final follow-up date. The normal control tissue was obtained as far as possible from the bump. All of the harvested specimens were cared for and manipulated according to the Declaration of Helsinki.

### Animal studies

As experimental animals, both male and female mice were used in this study. Four- to six-week old nude mice were purchased from Taconic (Taconic #NCR-NU) and housed in pathogen-free conditions. All animal experiments were strictly carried out following the protocol approved by the Institutional Animal Care and Use Committee (IACUC) at the Virginia Commonwealth University. For subcutaneous xenograft model, UM-SCC1 cells stably expressing FOSL1-shRNA or control Scr-shRNA were mixed with Matrigel and subcutaneously injected into the flank regions of the nude mice. The length and width of the tumor were routinely monitored and measured with a caliper every 3 days before the end point. The tumor volume was then calculated by the following formula: TV = (TL/TW<sup>2</sup>)/2 (where TV is tumor volume, TL is tumor length, and TW is tumor width). The tumors were removed after the mice were sacrificed. The weight of the tumors was recorded before histological examination. The frequency of HNSCC CSCs was calculated with ELDA software (<http://bioinf.wehi.edu.au/software/elda/index.html>) provided by the Walter and Eliza Hall Institute.<sup>66</sup> For the HNSCC orthotopic xenograft model, the indicated cells were injected into the tongue of nude mice. The tumor volume was then calculated, and the LNs were harvested and assessed. The use of human HNSCC PDX samples for this study was approved by the VCU Institutional Review Board. The human HNSCC PDX samples were obtained from the NCI Patient-Derived Models Repository (patient ID: 394591; specimen ID: 219-R). The HNSCC PDXs were maintained in *NOD-SCID* mice. For SR11302 administration, the HNSCC orthotopic xenograft model was established through inoculation of 10<sup>6</sup> tumor cells isolated from HNSCC PDX tumors (obtained from *NOD-SCID* mice) into the tongue of nude mice. Two weeks after inoculation with PDX tumor cells, the tumor-bearing mice were randomly divided into two groups. The treatment group was intraperitoneally injected with SR11302 10 mg/kg daily, and the control group was injected with only vehicle for

14 days. The mice were sacrificed at the end point, and tumors were dissected and weighed. The LNs were harvested and assessed in the orthotopic xenograft model. Toxicology studies were performed with C57BL/6 wild-type mice. The treatment group was intraperitoneally injected with SR11302 10 mg/kg daily, and the control group was injected with only vehicle for 14 days. The mice were sacrificed at the end point. Blood was collected for blood routine and biochemical index analysis. The major organs were also collected for IHC analysis.

#### **qRT-PCR and RNA-seq**

Total RNA was isolated from cells with the NucleoSpin RNA II RNA purification kit (Machery-Nagel; #740955.20). RNA concentrations were measured with NanoDrop One (Fisher Scientific). For qRT-PCR, cDNA was synthesized from 800 ng of total RNA with random primers and M-MuLV Reverse Transcriptase (New England Biolabs; #M0253L). Quantification of mRNA was determined with a SYBRGreen supermix (Bio-Rad; #1708880) on a CFX Connect Real-Time PCR Detection System (Bio-Rad). GAPDH levels were used as a loading control for real-time PCR. The primer sequences used for qRT-PCR are as listed in [Table S1](#). For RNA-seq, library preparation and sequencing were performed via the GENEWIZ RNA-seq service (GENEWIZ, South Plainfield, NJ, USA). The sequencing reads were first mapped to the hg19 UCSC transcript set with Bowtie 2 version 2.1.0, and the gene expression level was estimated with RSEM v1.2.15. Differentially expressed genes were identified with the edgeR program. Genes showing altered expression with  $p < 0.05$  and  $>1.5$ -fold changes were considered differentially expressed. GSEA and the statistical analyses were performed with GSEA software (<https://www.broadinstitute.org/GSEA>) and a two-tailed t test, respectively.

#### **ChIP-quantitative real-time PCR, ChIP-seq, and SE analysis**

For each ChIP reaction mixture,  $\sim 10^6$  cells were used. HNSCC cells were treated with 10 mM dimethyl 3,3'-dithiobispropionimidate-HCl (DTBP) (Thermo Fisher, #20665) in PBS at room temperature for 10 min and then fixed with 1% formaldehyde at 37°C for 10 min. Total cell lysates were sonicated to generate 200- to 400-bp DNA fragments. Chromatin complexes were immunoprecipitated with the following antibodies: anti-MED1 (Bethyl, #A300-793A), anti-FOSL1 (Cell Signaling, #5281). The precipitated DNA samples were measured by quantitative real-time PCR. Data are expressed as the percentage of input DNA. The primer sequences used for ChIP-quantitative real-time PCR are listed in [Table S2](#).

ChIP-seq libraries were generated with the NEBNext Ultra II DNA Library Prep Kit (NEB, #E7103S) according to the manufacturer's instructions. The workflow involved purification of ChIP DNA, end repair, A-tailing, adaptor ligation, and PCR amplification according to the manufacturer's instruction. NEB adaptors were used for multiplexing samples (NEB, NEBNext Multiplex Oligos for Illumina, #E7335S). The library samples were sequenced on Illumina HiSeq 3000 for a single read 50 run. Demultiplexing was performed with the Illumina Bcl2fastq2 v 2.17 program. Trimmomatic

was used to remove adaptors and to trim quality bases. We also eliminated leading, trailing ambiguous, and low-quality bases after adaptor clipping. Quality assessment confirmed that the ChIP-seq libraries meet the requirements of ENCODE standards. Bowtie was used to align the reads to the GRCh37 (hg19) human reference genome. Only uniquely mapped reads were used for the following downstream peak calling analysis. We used MACS2 for peak calling of the aligned data with default parameters ( $p$  value  $< 10^{-4}$ ). The respective input samples were used as background. The bamCoverage utility in deepTools was used to convert the bam to bigwig files. R package ChIPseeker was used for the peak annotation. To assign ChIP-seq enriched regions (peaks) to genes, we employed the cis-regulatory elements annotation system (CEAS) to create average profiling of all RefSeq genes and overlaps of significant peaks with genomic annotation regions. Genes with significant peaks within 5 kb of their TSSs were considered as bound. We used HOMER to find the most enriched motifs in a given peak set.

SEs were identified with ROSE software ([https://bitbucket.org/young\\_computation/rose](https://bitbucket.org/young_computation/rose)). In brief, the MED1 peaks within 12.5 kb of each other were stitched together as enhancer clusters. Enhancer clusters were then ranked and plotted based on each MED1 ChIP-seq signal. Stitched enhancer clusters that passed the inflection point in the distribution were designated as SEs. Peaks were excluded if they were entirely contained within  $\pm 2$  kb from a RefSeq TSS. Enhancers were assigned to the RefSeq transcript whose TSS was nearest to the center of the enhancer. The intersect utility in bedtools was used to calculate the overlapping of the SEs with other SEs or enhancers. The minimum overlap requirement is 1 bp. The SE- and TE-related genes were identified with the ROSE\_geneMapper command in the ROSE software. The t test was applied to compare the fold change of SE-associated genes and TE-associated genes.

#### **Co-immunoprecipitation and western blotting**

For nuclear IP,  $1 \times 10^7$  UM-SCC1 cells were used to prepare the nuclear extract. The nuclear extract was then incubated with antibodies or control immunoglobulin G (IgG) at 4°C overnight, followed by incubation with Dynabeads Protein G (Thermo Fisher) for 2 h. The beads were washed with PBS + 0.1% NP-40 three times at 4°C. Proteins bound to the beads were eluted with SDS loading buffer at 98°C for 5 min and then subjected to SDS-PAGE followed by western blotting analysis. For western blotting analysis, the total protein was extracted after lysis of cells with CelLytic buffer (Sigma-Aldrich, #C3228). The protein extracts were then loaded into SDS-PAGE with SDS loading buffer. The protein was then transferred into a polyvinylidene fluoride (PVDF) membrane after separation. The membranes were then immersed in 5% milk for blocking of nonspecific binding for 1 h. The membranes were then incubated with primary and secondary antibodies. The overnight incubation of primary antibody was followed by 2-h incubation of secondary antibody. The primary antibodies used in the present study were anti-FOSL1 (Cell Signaling, #5281), anti- $\alpha$ -Tubulin (Sigma Aldrich; #T9026), anti-CD44 (Cell Signaling, #3750), anti-CDH1 (Cell Signaling, #3195), anti-CDH2 (Cell Signaling, #13116), and anti-SNAI2 (Cell Signaling,

#9585). The membrane was then developed for chemiluminescence, and the images were recorded accordingly.

#### **Wound healing assay and cell migration and invasion assay**

For the wound healing assay, cells were seeded and incubated overnight. The next day, a wound was scratched in the cell layer with a sterile micropipette tip. Cells were then imaged daily with a microscope until the wound closed in the control group. Data were collected via ImageJ analysis. Similar experiments were also performed in cells pretreated with mitomycin C (10 µg/mL). The *in vitro* cell migration and invasion were measured with the Corning BioCoat Matrigel Invasion Chamber (Corning; #354480) according to the manufacturer's instructions. In brief, cells were seeded in the upper chambers, and culture medium with 1% FBS was added to the lower chambers. After 24 h of incubation, cells that migrated to the reverse side of inserts were stained with the Hema 3 Staining Kit (Fisher, #123-869) and quantified with ImageJ analysis.

#### **Flow cytometry and tumor sphere formation assay**

For flow cytometry analysis, the cell suspension of UM-SCC1 or FaDu cells was filtered through a 40-µm mesh filter. Subsequently, tumor cells were stained with the ALDEFLUOR assay kit (STEMCELL Technologies; #01700) according to the manufacturer's guidelines to label the ALDH<sup>high</sup> populations, followed by incubation of anti-CD44-APC antibody (Miltenyi Biotec, #130-113-893). The ALDEFLUOR-stained cells were treated with diethylaminobenzaldehyde, a specific ALDH inhibitor, to serve as ALDH-negative controls. For isolation of tumor cells from PDXs, ~6–8 weeks after implantation the xenograft tumors were isolated from mice, minced, and dissociated with the Tumor Dissociation Kit (Miltenyi Biotec, #130-095-929), and the tumor cells were subsequently isolated with the Tumor Cell Isolation Kit (Miltenyi Biotec, #130-108-339). For tumor sphere formation assays using CSCs, ALDH<sup>high</sup>/CD44<sup>high</sup> cells were sorted with a fluorescence-activated cell sorter (FACSAria III, BD Immunocytometry Systems). The isolated cells were cultured in ultra-low attachment plates at a density of 5,000 cells/well in serum-free DMEM/F12 (Fisher Scientific, #11330-032) supplemented with 1% B27 supplement (Fisher Scientific, #17504044), 1% N2 supplement (Fisher Scientific, #17502048), penicillin-streptomycin (100 µg/mL; Fisher Scientific, #15140122), human recombinant EGF (20 ng/mL; R&D Systems, #236-EG-01M), and human recombinant basic fibroblast growth factor (bFGF, 10 ng/mL; R&D Systems, #233-FB-025/CF) in a humidified 5% CO<sub>2</sub> incubator at 37°C. Fresh medium was replenished every 3 days. The number of the valid spheres was assessed under microscopy 1 week after plating. For *in vitro* sphere formation assays, 1,000 UM-SCC1 cells stably expressing SNAI2 or control cells were dissociated into single cells and seeded into 6-well plates, followed by siRNA transfection. The number of the valid spheres was assessed under microscopy 2 weeks after plating. For *in vitro* sphere formation with limiting dilution assays, HNSCC cells were dissociated into single cells and seeded into 96-well plates at the indicated cell doses. For each cell dose, at least 24 wells were seeded with cells. Fresh medium was replenished every 3 days. Two weeks later, sphere number was counted and the frequency of sphere-forming units was calculated with ELDA software.

#### **Immunohistochemistry**

IHC assays were performed with the VECTASTAIN Elite ABC Kit (Vector, #PK-6101) according to the manufacturer's guidelines and quantified as previously described.<sup>55,67</sup> The antibodies used in IHC assays were anti-FOSL1 (Cell Signaling, #5281), anti-Pan-Keratin (Cell Signaling, #4545), and anti-SNAI2 (Cell Signaling, #9585). The IHC score was calculated with the formula  $1 \times (\text{percentage of cells staining weakly}) + 2 \times (\text{percentage of cells staining moderately}) + 3 \times (\text{percentage of cells staining strongly})$  as previously described.<sup>67</sup>

#### **WGCNA and GSEA based on TCGA data sets**

RNA-seq and clinical data of the HNSCC from TCGA were downloaded with the UCSC Xena browser (<https://xenabrowser.net>). Patients with HNSCC who were followed up after >1 month were subjected to survival analysis based on their gene expression data. The gene expression data and survival results were used for the overall survival analysis. The top 50% of the genes with the largest variance in the HNSCC samples (9,829 genes) were used for WGCNA. All these processes were performed with R software (R version 3.5.3) and related R packages. The WGCNA package was applied to construct weighted gene correlation network analysis.<sup>68</sup> The outlier samples were removed by applying the goodSamplesGenes function and the hclust function ( $Z.k < \text{threshold}Z.k = 2.5$ ). A soft threshold  $\beta$  was selected to make the gene distribution conform to the scale-free network. After the  $\beta$  value was determined, the correlation matrix was transformed into an adjacency matrix with the adjacency function. Then, the TOMsimilarity function was used to convert the adjacency matrix into a topological overlap matrix, from which the corresponding dissimilarity was calculated. The dynamic cut tree method was used to perform hierarchical clustering according to the dissimilarity between genes to obtain a clustering tree, where different branches represent different gene modules (the module's minimum gene number is 30). The module eigengene represented the expression data of the genes contained in a module, and the gene modules could be clustered again by using the moduleEigengenes function. Then, the mergeCloseModules function was used to merge the gene modules whose dissimilarity is <0.2. The expression levels of each module eigengene were calculated to identify the modules that were significantly related to the expression of FOSL1. Finally, GO analysis was performed for the genes in the key modules.

GSEA was conducted between the high FOSL1 expression and low FOSL1 expression groups by using R package "clusterProfiler." The association of FOSL1 expression with oncogenetic biological function was performed with the Hallmark gene sets and curated gene sets (<https://www.gsea-msigdb.org/gsea/index.jsp>). A p value of <0.05 and a false discovery rate (FDR) of <0.05 for a gene set were considered statistically significant.

#### **Statistical analysis**

The results were presented as the mean ± SD from replicated experiments unless otherwise indicated. Two-tailed Student's t test was performed between two groups, and a difference was considered

statistically significant with  $p < 0.05$  with Prism 6 (GraphPad Software). Unpaired 2-tailed Student's t test was used to compare the means of 2 groups. Fisher's exact test was used to compare the difference between two categorical variables with Prism 6.

### Data availability

The accession numbers for the RNA-seq and ChIP-seq data reported in this paper are NCBI GEO: GSE151128 and GSE151132.

### SUPPLEMENTAL INFORMATION

Supplemental information can be found online at <https://doi.org/10.1016/j.ymthe.2021.03.024>.

### ACKNOWLEDGMENTS

This work was partially supported by an NIH/NIDCR grant (R03DE026822); the Elsa U. Pardee Foundation Award; the 2020 VCU Presidential Research Quest Fund; a VCU Massey Cancer Center Multi-Investigator Award (2019-MIP-05); and the 2020 VCU CCTR Endowment Fund (sub-award of UL1TR002649 from National Center for Advancing Translational Sciences to VCU's CTSA) to J.L., and National Natural Science Foundation of China (82073265 and 81572661); Natural Science Foundation of Guangdong Province (2017A030313515); and Guangdong Financial Fund for High-Caliber Hospital Construction (174-2018-XMZC-0001-03-0125/D-14) to C.W.

### AUTHOR CONTRIBUTIONS

The study was conceived and designed by J.L. and C.W. J.L. and C.W. developed the methodology. J.L., C.W., M.Z., R.G.H., Z.M., B.S., H.C., W.C., N.X., Y.Z., J.H., and X.L. acquired data (e.g., animals, IHC staining, specimens, sequencing). J.L., C.W., Z.M., R.G.H., and H.C. analyzed and interpreted the data (e.g., statistical analysis, biostatistics, and computational analysis). The manuscript was written by J.L. and C.W. with input from G.E.K., R.G.H., Y.S., and H.H. J.L. and C.W. supervised the study.

### DECLARATION OF INTERESTS

The authors declare no competing interests.

### REFERENCES

1. Siegel, R.L., Miller, K.D., and Jemal, A. (2015). Cancer statistics, 2015. *CA Cancer J. Clin.* **65**, 5–29.
2. Whyte, W.A., Orlando, D.A., Hnisz, D., Abraham, B.J., Lin, C.Y., Kagey, M.H., Rahl, P.B., Lee, T.I., and Young, R.A. (2013). Master transcription factors and mediator establish super-enhancers at key cell identity genes. *Cell* **153**, 307–319.
3. Hnisz, D., Abraham, B.J., Lee, T.I., Lau, A., Saint-André, V., Sigova, A.A., Hoke, H.A., and Young, R.A. (2013). Super-enhancers in the control of cell identity and disease. *Cell* **155**, 934–947.
4. Chipumuro, E., Marco, E., Christensen, C.L., Kwiatkowski, N., Zhang, T., Hatheway, C.M., Abraham, B.J., Sharma, B., Yeung, C., Altabef, A., et al. (2014). CDK7 inhibition suppresses super-enhancer-linked oncogenic transcription in MYCN-driven cancer. *Cell* **159**, 1126–1139.
5. Jang, M.K., Mochizuki, K., Zhou, M., Jeong, H.S., Brady, J.N., and Ozato, K. (2005). The bromodomain protein Brd4 is a positive regulatory component of P-TEFb and stimulates RNA polymerase II-dependent transcription. *Mol. Cell* **19**, 523–534.
6. Shi, J., and Vakoc, C.R. (2014). The mechanisms behind the therapeutic activity of BET bromodomain inhibition. *Mol. Cell* **54**, 728–736.
7. Lovén, J., Hoke, H.A., Lin, C.Y., Lau, A., Orlando, D.A., Vakoc, C.R., Bradner, J.E., Lee, T.I., and Young, R.A. (2013). Selective inhibition of tumor oncogenes by disruption of super-enhancers. *Cell* **153**, 320–334.
8. Rasool, R.U., Natesan, R., Deng, Q., Aras, S., Lal, P., Sander Effron, S., Mitchell-Velasquez, E., Posimo, J.M., Carskadon, S., Baca, S.C., et al. (2019). CDK7 Inhibition Suppresses Castration-Resistant Prostate Cancer through MED1 Inactivation. *Cancer Discov.* **9**, 1538–1555.
9. Roe, J.S., Mercan, F., Rivera, K., Pappin, D.J., and Vakoc, C.R. (2015). BET Bromodomain Inhibition Suppresses the Function of Hematopoietic Transcription Factors in Acute Myeloid Leukemia. *Mol. Cell* **58**, 1028–1039.
10. Devaiah, B.N., Gegonne, A., and Singer, D.S. (2016). Bromodomain 4: a cellular Swiss army knife. *J. Leukoc. Biol.* **100**, 679–686.
11. Alqahtani, A., Chouair, K., Ashraf, M., Hammouda, D.M., Allogabi, A., Khan, T., Senzer, N., and Nemunaitis, J. (2019). Bromodomain and extra-terminal motif inhibitors: a review of preclinical and clinical advances in cancer therapy. *Future Sci. OA* **5**, FSO372.
12. Pervaiz, M., Mishra, P., and Günther, S. (2018). Bromodomain Drug Discovery - the Past, the Present, and the Future. *Chem. Rec.* **18**, 1808–1817.
13. Stathis, A., and Bertoni, F. (2018). BET Proteins as Targets for Anticancer Treatment. *Cancer Discov.* **8**, 24–36.
14. Eckert, R.L., Adhikary, G., Young, C.A., Jans, R., Crish, J.F., Xu, W., and Rorke, E.A. (2013). AP1 transcription factors in epidermal differentiation and skin cancer. *J. Skin Cancer* **2013**, 537028.
15. Lopez-Bergami, P., Lau, E., and Ronai, Z. (2010). Emerging roles of ATF2 and the dynamic AP1 network in cancer. *Nat. Rev. Cancer* **10**, 65–76.
16. Shaulian, E., and Karin, M. (2002). AP-1 as a regulator of cell life and death. *Nat. Cell Biol.* **4**, E131–E136.
17. Ding, X., Pan, H., Li, J., Zhong, Q., Chen, X., Dry, S.M., and Wang, C.Y. (2013). Epigenetic activation of AP1 promotes squamous cell carcinoma metastasis. *Sci. Signal.* **6**, 1–13, ra28.
18. Jin, Y., Wang, C., Liu, X., Mu, W., Chen, Z., Yu, D., Wang, A., Dai, Y., and Zhou, X. (2011). Molecular characterization of the microRNA-138-Fos-like antigen 1 (FOSL1) regulatory module in squamous cell carcinoma. *J. Biol. Chem.* **286**, 40104–40109.
19. Zhang, X., Wu, J., Luo, S., Lechner, T., and Zhang, J.Y. (2016). FRA1 promotes squamous cell carcinoma growth and metastasis through distinct AKT and c-Jun dependent mechanisms. *Oncotarget* **7**, 34371–34383.
20. Chen, D., Wu, M., Li, Y., Chang, I., Yuan, Q., Ekimyan-Salvo, M., Deng, P., Yu, B., Yu, Y., Dong, J., et al. (2017). Targeting BMI1<sup>+</sup> Cancer Stem Cells Overcomes Chemoresistance and Inhibits Metastases in Squamous Cell Carcinoma. *Cell Stem Cell* **20**, 621–634.e6.
21. Wang, C., Liu, X., Huang, H., Ma, H., Cai, W., Hou, J., Huang, L., Dai, Y., Yu, T., and Zhou, X. (2012). Dereulation of Snai2 is associated with metastasis and poor prognosis in tongue squamous cell carcinoma. *Int. J. Cancer* **130**, 2249–2258.
22. Boxberg, M., Götz, C., Haidari, S., Dorfner, C., Jesinghaus, M., Drecoll, E., Boskov, M., Wolff, K.D., Weichert, W., Haller, B., and Kolk, A. (2018). Immunohistochemical expression of CD44 in oral squamous cell carcinoma in relation to histomorphological parameters and clinicopathological factors. *Histopathology* **73**, 559–572.
23. Wang, C., Huang, H., Huang, Z., Wang, A., Chen, X., Huang, L., Zhou, X., and Liu, X. (2011). Tumor budding correlates with poor prognosis and epithelial-mesenchymal transition in tongue squamous cell carcinoma. *J. Oral Pathol. Med.* **40**, 545–551.
24. Xie, N., Yu, P., Liu, H., Liu, X., Hou, J., Chen, X., Huang, H., and Wang, C. (2019). Validation of the International Tumor Budding Consensus Conference (2016) recommendations in oral tongue squamous cell carcinoma. *J. Oral Pathol. Med.* **48**, 451–458.
25. Mistry, D.S., Chen, Y., Wang, Y., Zhang, K., and Sen, G.L. (2014). SNAI2 controls the undifferentiated state of human epidermal progenitor cells. *Stem Cells* **32**, 3209–3218.
26. Wang, H., and Unternehrer, J.J. (2019). Epithelial-mesenchymal Transition and Cancer Stem Cells: At the Crossroads of Differentiation and Dedifferentiation. *Dev. Dyn.* **248**, 10–20.

27. Yilmaz, M., and Christofori, G. (2009). EMT, the cytoskeleton, and cancer cell invasion. *Cancer Metastasis Rev.* **28**, 15–33.
28. Hall, A. (2009). The cytoskeleton and cancer. *Cancer Metastasis Rev.* **28**, 5–14.
29. Fife, C.M., McCarroll, J.A., and Kavallaris, M. (2014). Movers and shakers: cell cytoskeleton in cancer metastasis. *Br. J. Pharmacol.* **171**, 5507–5523.
30. Major, A.G., Pitty, L.P., and Farah, C.S. (2013). Cancer stem cell markers in head and neck squamous cell carcinoma. *Stem Cells Int.* **2013**, 319489.
31. Singh, A., and Settleman, J. (2010). EMT, cancer stem cells and drug resistance: an emerging axis of evil in the war on cancer. *Oncogene* **29**, 4741–4751.
32. Shibue, T., and Weinberg, R.A. (2017). EMT, CSCs, and drug resistance: the mechanistic link and clinical implications. *Nat. Rev. Clin. Oncol.* **14**, 611–629.
33. Dongre, A., and Weinberg, R.A. (2019). New insights into the mechanisms of epithelial-mesenchymal transition and implications for cancer. *Nat. Rev. Mol. Cell Biol.* **20**, 69–84.
34. Puram, S.V., Tirosh, I., Parikh, A.S., Patel, A.P., Yizhak, K., Gillespie, S., Rodman, C., Luo, C.L., Mroz, E.A., Emerick, K.S., et al. (2017). Single-Cell Transcriptomic Analysis of Primary and Metastatic Tumor Ecosystems in Head and Neck Cancer. *Cell* **171**, 1611–1624.e24.
35. Weinstein, I.B. (2002). Cancer. Addiction to oncogenes—the Achilles heel of cancer. *Science* **297**, 63–64.
36. Kirk, R. (2011). Targeted therapies: model reveals addiction to oncogenes. *Nat. Rev. Clin. Oncol.* **8**, 691.
37. Yang, H.W., Menon, L.G., Black, P.M., Carroll, R.S., and Johnson, M.D. (2010). SNAI2/Slug promotes growth and invasion in human gliomas. *BMC Cancer* **10**, 301.
38. Ota, I., Masui, T., Kurihara, M., Yook, J.I., Mikami, S., Kimura, T., Shimada, K., Konishi, N., Yane, K., Yamanaka, T., and Kitahara, T. (2016). Snail-induced EMT promotes cancer stem cell-like properties in head and neck cancer cells. *Oncol. Rep.* **35**, 261–266.
39. Binda, E., Visioli, A., Giani, F., Lamorte, G., Copetti, M., Pitter, K.L., Huse, J.T., Cajola, L., Zanetti, N., DiMeco, F., et al. (2012). The EphA2 receptor drives self-renewal and tumorigenicity in stem-like tumor-propagating cells from human glioblastomas. *Cancer Cell* **22**, 765–780.
40. Huang, C., Ma, W.Y., Dawson, M.I., Rincon, M., Flavell, R.A., and Dong, Z. (1997). Blocking activator protein-1 activity, but not activating retinoic acid response element, is required for the antitumor promotion effect of retinoic acid. *Proc. Natl. Acad. Sci. USA* **94**, 5826–5830.
41. Sun, Y., Lin, Z., Liu, C.H., Gong, Y., Liegl, R., Fredrick, T.W., Meng, S.S., Burnim, S.B., Wang, Z., Akula, J.D., et al. (2017). Inflammatory signals from photoreceptor modulate pathological retinal angiogenesis via c-Fos. *J. Exp. Med.* **214**, 1753–1767.
42. Fanjul, A., Dawson, M.I., Hobbs, P.D., Jong, L., Cameron, J.F., Harlev, E., Graupner, G., Lu, X.P., and Pfahl, M. (1994). A new class of retinoids with selective inhibition of AP-1 inhibits proliferation. *Nature* **372**, 107–111.
43. Park, M.J., Moon, S.J., Lee, S.H., Kim, E.K., Yang, E.J., Min, J.K., Park, S.H., Kim, H.Y., Yang, C.W., and Cho, M.L. (2014). Blocking activator protein 1 activity in donor cells reduces severity of acute graft-versus-host disease through reciprocal regulation of IL-17-producing T cells/regulatory T cells. *Biol. Blood Marrow Transplant.* **20**, 1112–1120.
44. Oruqaj, G., Karnati, S., Vijayan, V., Kotarkonda, L.K., Boateng, E., Zhang, W., Ruppert, C., Günther, A., Shi, W., and Baumgart-Vogt, E. (2015). Compromised peroxisomes in idiopathic pulmonary fibrosis, a vicious cycle inducing a higher fibrotic response via TGF-β signaling. *Proc. Natl. Acad. Sci. USA* **112**, E2048–E2057.
45. Mishra, D.K., and Kim, M.P. (2017). SR 11302, an AP-1 Inhibitor, Reduces Metastatic Lesion Formation in Ex Vivo 4D Lung Cancer Model. *Cancer Microenviron.* **10**, 95–103.
46. Dawson, M.A., and Kouzarides, T. (2012). Cancer epigenetics: from mechanism to therapy. *Cell* **150**, 12–27.
47. Asangani, I.A., Dommetti, V.L., Wang, X., Malik, R., Cieslik, M., Yang, R., Escar-Wilke, J., Wilder-Romans, K., Dhanireddy, S., Engelke, C., et al. (2014). Therapeutic targeting of BET bromodomain proteins in castration-resistant prostate cancer. *Nature* **510**, 278–282.
48. Wajapeyee, N., Malonia, S.K., Palakurthy, R.K., and Green, M.R. (2013). Oncogenic RAS directs silencing of tumor suppressor genes through ordered recruitment of transcriptional repressors. *Genes Dev.* **27**, 2221–2226.
49. Shaulian, E. (2010). AP-1—The Jun proteins: Oncogenes or tumor suppressors in disguise? *Cell. Signal.* **22**, 894–899.
50. Thiery, J.P., Acloque, H., Huang, R.Y., and Nieto, M.A. (2009). Epithelial-mesenchymal transitions in development and disease. *Cell* **139**, 871–890.
51. De Craene, B., and Berx, G. (2013). Regulatory networks defining EMT during cancer initiation and progression. *Nat. Rev. Cancer* **13**, 97–110.
52. Guo, W., Keckesova, Z., Donaher, J.L., Shibue, T., Tischler, V., Reinhardt, F., Itzkovitz, S., Noske, A., Zürcher-Härdi, U., Bell, G., et al. (2012). Slug and Sox9 cooperatively determine the mammary stem cell state. *Cell* **148**, 1015–1028.
53. Luanpitpong, S., Li, J., Manke, A., Brundage, K., Ellis, E., McLaughlin, S.L., Angsutararux, P., Chanthra, N., Voronkova, M., Chen, Y.C., et al. (2016). SLUG is required for SOX9 stabilization and functions to promote cancer stem cells and metastasis in human lung carcinoma. *Oncogene* **35**, 2824–2833.
54. Chung, M.K., Jung, Y.H., Lee, J.K., Cho, S.Y., Murillo-Sauca, O., Uppaluri, R., Shin, J.H., and Sunwoo, J.B. (2018). CD271 Confers an Invasive and Metastatic Phenotype of Head and Neck Squamous Cell Carcinoma through the Upregulation of Slug. *Clin. Cancer Res.* **24**, 674–683.
55. Zhuang, Z., Yu, P., Xie, N., Wu, Y., Liu, H., Zhang, M., Tao, Y., Wang, W., Yin, H., Zou, B., et al. (2020). MicroRNA-204-5p is a tumor suppressor and potential therapeutic target in head and neck squamous cell carcinoma. *Theranostics* **10**, 1433–1453.
56. Liu, S., Shi, L., Wang, Y., Ye, D., Ju, H., Ma, H., Yang, W., Wang, Y., Hu, J., Deng, J., and Zhang, Z. (2018). Stabilization of Slug by NF-κB is Essential for TNF-α -Induced Migration and Epithelial-Mesenchymal Transition in Head and Neck Squamous Cell Carcinoma Cells. *Cell. Physiol. Biochem.* **47**, 567–578.
57. Angel, P., Hattori, K., Smeal, T., and Karin, M. (1988). The jun proto-oncogene is positively autoregulated by its product, Jun/AP-1. *Cell* **55**, 875–885.
58. Vial, E., and Marshall, C.J. (2003). Elevated ERK-MAP kinase activity protects the FOS family member FRA-1 against proteasomal degradation in colon carcinoma cells. *J. Cell Sci.* **116**, 4957–4963.
59. Chen, C., Zhao, S., Karnad, A., and Freeman, J.W. (2018). The biology and role of CD44 in cancer progression: therapeutic implications. *J. Hematol. Oncol.* **11**, 64.
60. Kothapalli, D., Flowers, J., Xu, T., Puré, E., and Assoian, R.K. (2008). Differential activation of ERK and Rac mediates the proliferative and anti-proliferative effects of hyaluronan and CD44. *J. Biol. Chem.* **283**, 31823–31829.
61. Al-Hajj, M. (2007). Cancer stem cells and oncology therapeutics. *Curr. Opin. Oncol.* **19**, 61–64.
62. Valent, P., Bonnet, D., De Maria, R., Lapidot, T., Copland, M., Melo, J.V., Chomienne, C., Ishikawa, F., Schuringa, J.J., Stassi, G., et al. (2012). Cancer stem cell definitions and terminology: the devil is in the details. *Nat. Rev. Cancer* **12**, 767–775.
63. Vidal, S.J., Rodriguez-Bravo, V., Galsky, M., Cordon-Cardo, C., and Domingo-Domenech, J. (2014). Targeting cancer stem cells to suppress acquired chemotherapy resistance. *Oncogene* **33**, 4451–4463.
64. Yokoyama, Y., Zhu, H., Lee, J.H., Kossenkov, A.V., Wu, S.Y., Wickramasinghe, J.M., Yin, X., Palozola, K.C., Gardini, A., Showe, L.C., et al. (2016). BET Inhibitors Suppress ALDH Activity by Targeting ALDH1A1 Super-Enhancer in Ovarian Cancer. *Cancer Res.* **76**, 6320–6330.
65. Gimple, R.C., Kidwell, R.L., Kim, L.J.Y., Sun, T., Gromovsky, A.D., Wu, Q., Wolf, M., Lv, D., Bhargava, S., Jiang, L., et al. (2019). Glioma Stem Cell-Specific Superenhancer Promotes Polyunsaturated Fatty-Acid Synthesis to Support EGFR Signaling. *Cancer Discov.* **9**, 1248–1267.
66. Hu, Y., and Smyth, G.K. (2009). ELDA: extreme limiting dilution analysis for comparing depleted and enriched populations in stem cell and other assays. *J. Immunol. Methods* **347**, 70–78.
67. Pirker, R., Pereira, J.R., von Pawel, J., Krzakowski, M., Ramlau, R., Park, K., de Marinis, F., Eberhardt, W.E., Paz-Ares, L., Störkel, S., et al. (2012). EGFR expression as a predictor of survival for first-line chemotherapy plus cetuximab in patients with advanced non-small-cell lung cancer: analysis of data from the phase 3 FLEX study. *Lancet Oncol.* **13**, 33–42.
68. Langfelder, P., and Horvath, S. (2008). WGCNA: an R package for weighted correlation network analysis. *BMC Bioinformatics* **9**, 559.